Advanced Practical Course Environmental Physics

F52: Electromagnetic Methods in Applied Geophysics

Institute of Environmental Physics
Heidelberg University

Patrick Klenk, Stefan Jaumann and Lisa Hantschel

Version: May 2017

Contents

1 Safety during the experiment iii

2 Introduction 1

3 Soil Physics 5
- 3.1 Porous media . . . 5
- 3.2 Macroscopic state variables . . . 5
- 3.3 Hydraulic dynamics in the vadose zone . . . 6
- 3.4 Parameterizations . . . 8
  - 3.4.1 Soil water characteristic function . . . 9
  - 3.4.2 Concluding remarks . . . 12

4 Electromagnetics 13
- 4.1 Electromagnetic Wave Propagation in Matter . . . 13
  - 4.1.1 Maxwell's Equations and Preliminary Assumptions . . . 13
  - 4.1.2 The Electrical Conductivity . . . 13
  - 4.1.3 The Dielectric Permittivity . . . 14
  - 4.1.4 Propagation of Electromagnetic Waves . . . 16
- 4.2 Guided Waves - Transmission Line Theory . . . 17
- 4.3 Measuring Material Properties with Electromagnetic Waves . . . 18
  - 4.3.1 The Reflection Coefficient . . . 18
  - 4.3.2 Wavelet Concept . . . 18
- 4.4 The Relative Dielectric Permittivity of Soils . . . 19
  - 4.4.1 The Relative Permittivity of Water . . . 19

5 Petrophysical Relationship 21

6 Time Domain Reflectometry 23
- 6.1 Measurement Principle . . . 23
- 6.2 Evaluation of the TDR Signal . . . 24
- 6.3 Electrical Conductivity . . . 25
- 6.4 Measurement Volume . . . 26
- 6.5 Concluding Remarks . . . 27

7 Ground Penetrating Radar 29
- 7.1 Measurement Principle . . . 29
- 7.2 Measurement System . . . 32
- 7.3 Measurement Setups . . . 32

7.3.1 Common Offset (CO) . . . 32
7.3.2 Multi-channel GPR . . . 35
7.4 Energy Loss and Penetration Depth . . . 37
7.5 Signal Resolution . . . 38
7.6 Concluding Remarks . . . 39

8 Site Introduction: ASSESS-GPR 41
8.1 Construction and basic characteristics . . . 41
8.2 Exemplary GPR measurement . . . 42
8.3 Previous studies at ASSESS-GPR . . . 44
8.4 Alternate field site: Grenzhof . . . 45

9 Experiments 47
9.1 Structure and aims of the experiments . . . 47
9.2 Guiding questions . . . 47
9.3 Laboratory measurements using TDR . . . 49
9.3.1 Basics: Performing TDR measurements . . . 49
9.3.2 Calibration of TDR sensors . . . 50
9.3.3 Measurement: TDR signals from a sand column . . . 50
9.3.4 Measurement: Assessing the Influence of conductivity . . . 52
9.4 Field measurements . . . 53
9.4.1 Planning your measurement . . . 53
9.4.2 Measurements you will need for evaluation . . . 53
9.4.3 Executing GPR measurements with automated field scanner . . . 55

10 Evaluation 59
10.1 Evaluation of the TDR measurements . . . 59
10.1.1 Qualitative description of TDR signals . . . 59
10.1.2 TDR signals from the sand column . . . 59
10.1.3 Assessing the influence of conductivity . . . 59
10.1.4 TDR field data . . . 60
10.2 Evaluation of the GPR field measurements . . . 60
10.2.1 Evaluation of measured data . . . 60
10.2.2 Comparison between methods and to TDR data . . . 63

Bibliography 65

1 Safety during the experiment

For your own safety during the experiment, please read the following instructions carefully.

Safety instructions for TDR experiment:

- You are working in a lab also used for different experiments including chemicals. Therefore be careful when using some unknown material which does not belong to the TDR experiment
- Drinking and eating in labs is not allowed.
- Follow common savety instructions concerning the handling of batteries and voltage sources.

Safety instructions for GPR experiment:

- You are working on free field. Read the weather forecast and adjust your equipment according to the daily conditions. At every time of the year sunscreen, water and a hat are mandatory at sunny days and controlled before we leave the institute.
- Fhe ASSESS site is up to 2 m high, so falling down can lead to serious injuries. Use the stairs for moving up and downwards. Do not do any climbing at the concrete walls. Keep distance from the edges of the ASSES site. Do not move backwards close to the edges.
- Warn other persons located on the ASSESS site before executing measurements with the field scanner. One person always has to stay close to the emergency stop button during the measurements.
- Follow common safety instructions concerning the handeling of batteries and voltage sources.

2 Introduction

This practical course serves as an introduction to the scientific field of **soil hydrology**. Soil hydrology focuses primarily on understanding and predicting the water distribution and the movement of water and solutes in soils. In recent years, the field has profited a great deal from combining high-resolution, high-precision measurement methods with state-of the art numerical modeling and simulation tools. While advanced measurement methods allow for an ever more precise imaging of near-surface hydrologic processes, numerical modeling methods have been proven to be an invaluable tool for obtaining a consistent description of these observed water dynamics in soils.

Hence, two main aspects have emerged in the framework of this advanced practical course: (i) the modeling of soil water dynamics and (ii) its measurement both in the laboratory and in the field with geophysical methods. However, as the science and our group's capabilities advance, the material which we would like to convey to you throughout this course has outgrown the scope of one single practical field course. Hence, starting in 2015, this practical course has been divided into two parts, which can be occasionally combined into one double course:

F52: Electromagnetic Methods in Applied Geophysics This is the more experimental part of the course where a particular focus is on the application of two electromagnetic geophysical methods: time domain reflectometry (TDR) and more importantly ground penetrating radar (GPR). The first is a high-precision point scale method while the latter can also yield information about distinct subsurface structures.

F53: Numerical Modeling in Soil Physics In the framework of this part of the practical course, soil water dynamics is exploited as an exemplary working horse process in order to discuss methods for estimating effective material properties of non-linear processes in environmental physics. Naturally, the concepts presented here are directly transferrable to different non-linear models.

Both parts are intrinsically linked as they tackle shared research questions from different angles. Hence, you will benefit greatly from participating in both practical courses if you have a particular interest in the fields of soil physics, soil hydrology or hydrogeophysics. In any case you will notice, that large parts of the basic theory are shared between both manuals, including this introduction. Subsequently, you will learn more about the specifics of the employed experimental methods for F52, while the description of F53 turns to the details of modeling procedures instead.

Motivation

Water is important to sustain life on Earth as it is one limiting factor for plant growth and thus for the production of nutrients for animals and human beings.
Most of the world's food is produced with the help of irrigation of groundwater and fertilization. Since the time scale of groundwater renewal is several thousand years, it is vital to use the groundwater efficiently and to minimize its pollution with fertilizers. Evaporation, groundwater recharge, and solute transport depend strongly on the soil hydraulic material properties of the soil, which depend on the soil water content and vary over many orders of magnitude in a very non-linear way.
Thus, to optimize food production and fresh water consumption, the development of a fast and non-invasive method to determine soil hydraulic material properties is needed.

Measuring the Volumetric Water Content

There is a huge variety of methods, which aim to measure the water content of the soil. These methods can be distinguished in direct or indirect, in invasive or non-invasive techniques as well as concerning to the scale of their application. Here, indirect measurements are methods, where the water content is obtained via physical proxy quantities such as dielectric material properties. In the following only a few examples will be given to measure the soil water content.

The most prominent direct and invasive technique is the gravimetric method. Here, a previously extracted moist soil sample with a known volume is weighted, dried and weighted again. From this, one can obtain the gravimetric as well as the volumetric water content at a single point. Disadvantageously, this method is very time consuming, when studying the distribution of the water content at the field scale.

An example for an indirect and almost non-invasive techniques is the neutron probe, which can be installed in a borehole. Here, neutrons are emitted and transmitted through the soil sample of interest. The scattering of these neutrons depends on the amount of water in the soil. Unfortunately, this technique is again only applicable on a local scale and it is not completely without healthy risks for the operator.

Some measurement techniques of the soil water content are based on the dielectric method. Here, the dielectric permittivity of the soil is used as a proxy for the volumetric water content, because the relative permittivity of water ($\varepsilon_{\text{water}} \approx 80$) is significantly higher than of the soil matrix ($\varepsilon_{\text{matrix}} \approx 4-5$) and of the air ($\varepsilon_{\text{air}} = 1$) within the soil pore space. Examples for this class of techniques are the time domain reflectometry (TDR) and the ground penetrating radar (GPR), which will be applied in this practical course. For both methods, the travel time of either guided or free electromagnetic waves is measured, which is closely related to the relative permittivity of the medium via the electromagnetic wave velocity. Here, TDR can be recognized as a method for local measurements, where GPR is applied on the regional scale for water content measurements for a few tenth to hundreds

of meter survey length.

Acknowledgements

Over the years, several persons have added and expanded on this practical course script. We especially acknowledge contributions (in alphabetical order) by Jens S. Buchner, Holger Gerhards, Rebecca Ludwig and Ute Wollschläger.

3 Soil Physics

In this chapter, several fundamental concepts of soil physics are introduced which will be the foundation for explaining and modeling some of the hydraulic processes which may be observed in this field course. The aim of this section is not to present a comprehensive theory of soil physics as such, but to briefly outline a macroscopic description of the movement of water in soils based on few effective hydraulic parameters. Large parts of this section are taken from *Klenk* (2012), all considerations largely follow the much more in-depth treatment which can be found in the soil physics lecture notes by *Roth* (2012).

3.1 Porous media

Soil physics aims at describing the movement of water and solutes in the soil. A soil in this context can usually be characterized as a porous medium. Following *Roth* (2012), such a description of a soil as a porous medium assumes (i) a division of the total volume into soil matrix and pore space which is filled by one or more fluids, (ii) the existence of a characteristic length scale l, down to which each volume element consists of both soil matrix and pore space and (iii) the interconnectedness of the pore space for allowing the movement of water and solutes. The volume fraction of the pore space is denoted by the *porosity* ϕ.

3.2 Macroscopic state variables

A direct description of the properties of the porous medium is cumbersome and not conducive to the type of problems which will be addressed in the framework of this experiment. However, based on the existence of the characteristic length scale l, we can invoke the existence of a suitable averaging volume, a so-called Representative Elementary Volume (REV), containing all characteristic microscopic heterogeneities of the medium. Suitably averaging the microscopic quantities describing the properties at the pore scale over such a REV, the hydraulic state of the system can be described by two macroscopic state variables, the volumetric fluid content and the potential energy density of the respective phases. Neglecting the potential presence of solutes and assuming a constant temperature T, these state variables are determined by the height z and the pressure p_i in the respective phase i. In the context of this experiment we can restrict all following considerations to two phases, namely air and water. Then, the volumetric fluid contents

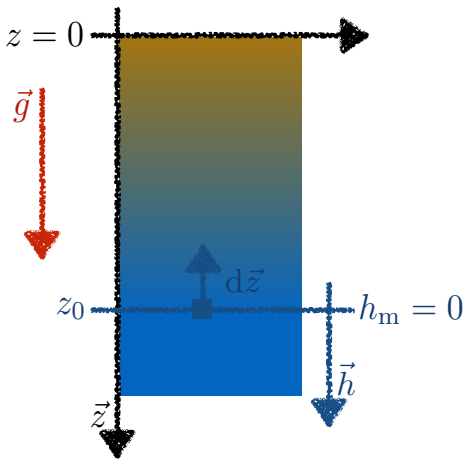

Figure 3.1: Convention of the axes orientation: The z-axis and the gravitation vector $\vec{g}$ are parallel and pointing downwards. At the surface z is equal to zero. The matrix potential h_m has to be zero at the position of the water table which located at z_0.

for air and water, θ_a and θ_w can be defined by:

$$\theta_i = \frac{V_i}{V}, \tag{3.1}$$

with V_i the volume of the respective fluid phase, and V denoting the total volume. The potential energy densities ψ_a and ψ_w are defined as the energy which would be needed for moving a unit's volume of this phase from a suitable reference state $\{p_0, z_0\}$ to a certain location within the porous medium characterized by $\{p_i, z\}$:

$$\psi_i(x) = p_i - p_0 + \int_{z_0}^{z} \vec{g}\, \rho_i(z')\, \mathrm{d}\vec{z}' = p_i - p_0 - \rho g(z - z_0). \tag{3.2}$$

A suitable $z = z_0$ can for instance represent the position of the water table or the deepest point in the considered profile; p_0 will in our case be assumed to be atmospheric pressure.

3.3 Hydraulic dynamics in the vadose zone

The vadose zone is commonly viewed as the unsaturated part of the soil profile above a ground water table. Assuming an arbitrarily mobile airphase, the movement of water can be described by a partial differential equation, the Richards equation, which will be derived in this section based on the conservation of mass and an empirical flux law.
An arbitrarily mobile airphase is a reasonable assumption for profile parts far away from the groundwater table where the air phase can be assumed to be continuous and connected to the atmosphere. In this case, the movement of air will be approximately instantaneous as compared to the movement of water. Hence we can assume $p_a = p_0$ and restrict our considerations to describing the movement of the water phase. This region is usually

denoted as the *degenerate multiphase regime*. With these assumptions and further assuming the incompressibility of water under these circumstances (i.e. $\rho_w = \text{const}$), the corresponding *soil water potential* ψ_w can be written, based on equation 3.2, as:

$$\psi_w = \psi_m + \psi_g = p_w - p_0 - \rho g(z - z_0) = p_w - p_a - \rho g(z - z_0), \tag{3.3}$$

with the matric potential

$$\psi_m = p_w - p_a, \tag{3.4}$$

and the gravitational potential

$$\psi_g = -\rho g(z - z_0). \tag{3.5}$$

From the definition 3.4 the matric potential will be negative for bound water (in the vadose zone) and positive for free water (e.g., in the ground water). At times it might be convenient to express the soil water potential in terms of height.
Dividing equation 3.3 by $\rho_w g$ yields the so-called *hydraulic head* h_w:

$$h_w = h_m - (z - z_0), \tag{3.6}$$

with the *matric head*

$$h_m = \frac{\psi_m}{\rho_w g} \tag{3.7}$$

describing the negative height above z_0 for the corresponding potential. For $z_0 = 0$ at the position of the water table, and equilibrium conditions ($h_w = 0$), $h_m = z$ holds.

The **conservation of mass** for a fluid phase i is given by:

$$\partial_t \left[\theta_i \rho_i\right] + \nabla \cdot \left[\rho_i \vec{j_i}\right] = 0, \tag{3.8}$$

with the macroscopic volume flux $\vec{j_i}$. Assuming again water to be incompressible (i.e. $\rho_w = \text{const}$), the conservation of water can be expressed accordingly:

$$\partial_t \theta_w + \nabla \cdot \vec{j_w} = 0, \tag{3.9}$$

with the water flux $\vec{j_w}$, as long as there is no explicit extraction of water from the considered volume (for example by pumping).
In porous media, a macroscopic volume flux can be described by an empirical macroscopic flux law, Darcy's law:

$$\vec{j_i} = -K_i \nabla \psi_i, \tag{3.10}$$

stating that a slow, stationary flux of a Newtonian fluid i will be proportional to the forcing by a potential gradient and directed in the negative direction of this gradient. For describing fluid movement in unsaturated porous media, this is supplemented by the Buckingham conjecture assuming that in this case the factor of proportionality K_i will

depend on the respective fluid content θ_i. This yields the **Buckingham-Darcy law**, which reads expressed for water flux:

$$\vec{j_w} = -K_w(\theta_w)\,\nabla\psi_w, \tag{3.11}$$

with the *hydraulic conductivity* $K_w(\theta_w)$. Hence, while the water movement in the ground water can be described by an approximately constant value, the hydraulic conductivity in the unsaturated zone $K_w(\theta_w)$ will be a strong function of water content.

Now, inserting equation 3.11 into equation 3.9 and using the relationship 3.3, this yields the **Richards equation**:

$$\partial_t\theta_w(\psi_m) - \nabla\cdot\left[K_w(\theta_w(\psi_m))\left[\nabla\psi_m - \rho g\right]\right] = 0, \tag{3.12}$$

which has first been formulated by *Richards* (1931). We have to reiterate that this equation has just been derived under the explicit assumptions of a degenerate multiphase regime, i.e. it is strictly only applicable for parts of the soil profile with sufficiently small water contents. This has to be kept in mind, especially for comparing numerical simulations and the results of measurements under conditions close to saturation.
equation 3.12 also acknowledges the strong dependency of the water content θ_w on the matric potential ψ_m. Hence, for solving this highly non-linear equation, it needs to be supplemented by constitutive relationships for the *soil water characteristic* $\theta_w(\psi_m)$ and the *hydraulic conductivity function* $K(\psi_m)$. These relationships are commonly supplied by different parameterization models which describe these relations for a given soil with a set of effective parameters. As will be shown in the following section, these parameters can in turn be associated with certain hydraulic properties of the studied system.

3.4 Parameterizations

The two most widely acknowledged models for these two constitutive relationships have been provided by Mualem-van Genuchten and Mualem-Brooks-Corey. Dropping the explicit subscript w, both models are most conveniently formulated in terms of the hydraulic head h_m and the water saturation Θ:

$$\Theta := \frac{\theta - \theta_r}{\theta_s - \theta_r}, \tag{3.13}$$

with saturated and residual water contents θ_s and θ_r, respectively. The saturated water content is in general not equal to the porosity ϕ of the medium, since depending in the specific conditions even at saturation the medium can retain some entrapped air. The residual water content describes the amount of water which cannot be simply removed from the medium by hydraulic processes, for example by applying a pressure gradient.

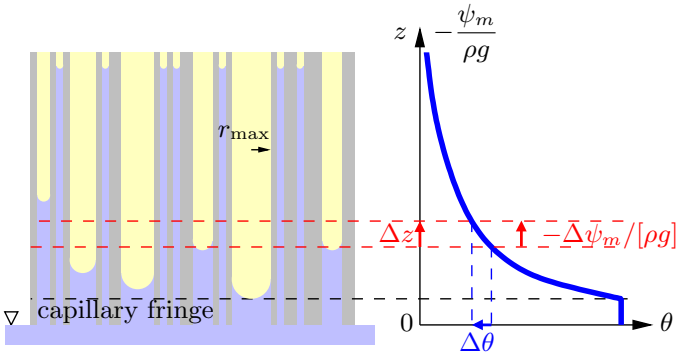

Figure 3.2: A simple model for the soil is a bundle of capillaries with a distribution of different radii. The largest radius determines the size of the capillary fringe.

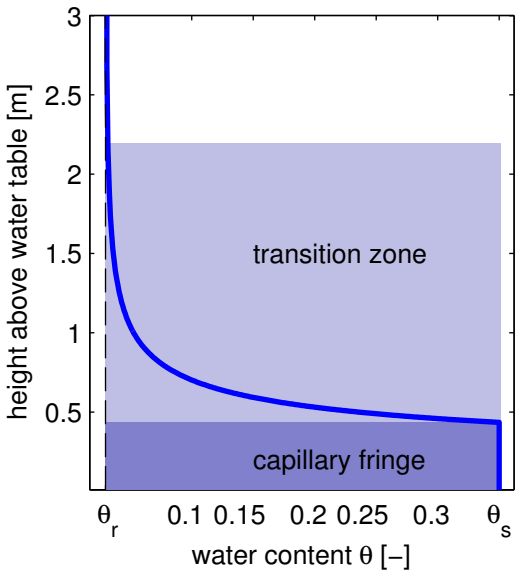

Figure 3.3: Soil water profile above a water table in a homogeneous sand in hydrostatic equilibrium

3.4.1 Soil water characteristic function

An apt formulation for the soil water characteristic function can be based on considering the porous medium as a bundle of equivalent capillaries. Assuming approximately spherical pores of radius r, the matric head can be related to the capillary pressure as given by the Young-Laplace law:

$$h_m = \frac{p_w - p_a}{\rho_w g} = \frac{-2\sigma_w}{r\rho_w g}, \tag{3.14}$$

with the interfacial energy density of water $\sigma_w = 0.0725\ {}^{\mathrm{N}}/_{\mathrm{m}^2}$.

Essentially this means that the size of the respective pores determines the strength with which the water is bound in the soil. Conversely, there is a certain maximum pore size for

a given matric head in which the water can still be held by capillary forces. When applying a larger pressure gradient, pores of this size will be drained. Hence, in a stationary profile, we will expect a certain region above the water table which will be held at saturation due to capillary forces. The extent of this **Capillary Fringe** is determined by the largest pores in the medium, which can sustain the smallest capillary rise.
Hence, the finer the material, the larger the expected height of the capillary fringe. Above the capillary fringe we can expect a gradual decrease of saturation towards the residual water content θ_r. In equilibrium, the shape of this transition zone will depend mainly on the variety of different pore sizes, i.e. the specific pore size distribution. The wider the pore size distribution, the more gradual the transition. For a very narrow pore size distribution all pores will drain for a very narrow range of pressure gradients, leading to a correspondingly rather small transition zone. Based on these considerations, one might envision the soil water characteristic in a form as has been drawn in figure 3.2.

There is a multitude of parameterizing models which characterize this system in the literature. The three most commonly applied models are the Brooks-Corey parameterization (*Brooks* (1966)), the van Genuchten parameterization and a simplified version of the latter (*Van Genuchten* (1980)). figure 3.3 has in fact been calculated based on the Brooks-Corey parameterization, which is given by:

$$\Theta\left(h_m\right) = \begin{cases} \left[-\frac{h_m}{h_0}\right]^{-\lambda}; & -h_m > h_0 \\ 1; & -h_m < h_0 \end{cases} \tag{3.15}$$

with the *air entry value* $h_0 > 0$ and the shape parameter λ. The more intuitive approach is to consider its inverse function, which is defined for $\Theta < 1$ as:

$$h_m\left(\Theta\right) = -h_0 \Theta^{-\frac{1}{\lambda}}. \tag{3.16}$$

In connection with equation 3.14, this formulation highlights the association of the air entry value h_0 with the largest available pores as discussed above, and the connection of the parameter λ to the shape of the transition zone above the capillary fringe (and in turn to the specifics of the pore size distribution). In general, h_0 can be viewed as a scaling factor since it has an influence on the shape of the transition zone, as has, e.g., been discussed in *Dagenbach* (2012).

For completeness, the general van Genuchten parameterization is given by:

$$\Theta\left(h_m\right) = \left[1 + \left[-\alpha h_m\right]^n\right]^{-m}, \tag{3.17}$$

with shape parameters $\alpha > 0$, $n > 1$ and $m > 0$. The corresponding inverse function can be expressed as:

$$h_m\left(\Theta\right) = -\frac{1}{\alpha}\left[\Theta^{-\frac{1}{m}} - 1\right]^{\frac{1}{n}}. \tag{3.18}$$

Setting $m = 1 - 1/n$ leads to the special case of the simplified van Genuchten parameterization with

$$\Theta\left(h_m\right) = \left[1 + \left[-\alpha h_m\right]^n\right]^{-1+1/n} \tag{3.19}$$

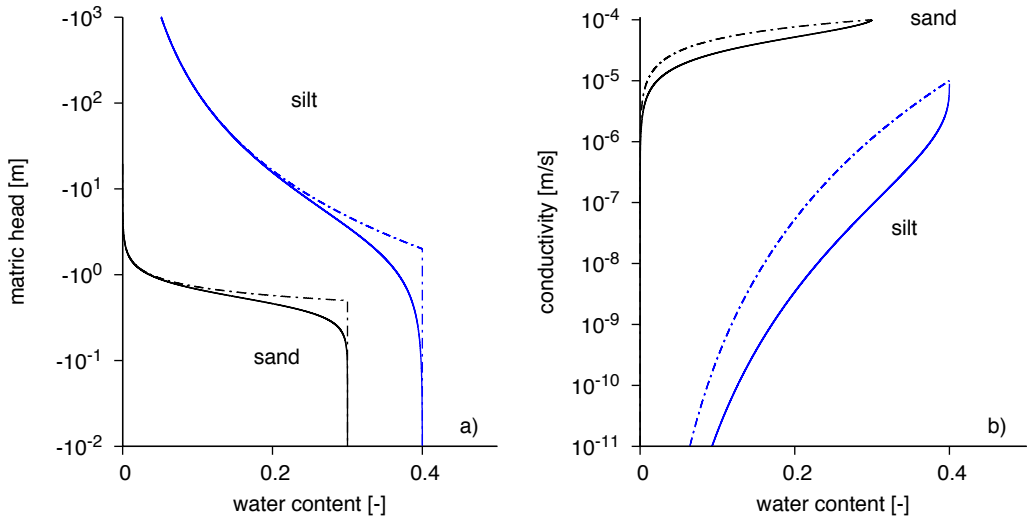

Figure 3.4: Soil water characteristic function $h(\theta)$ (left) and corresponding hydraulic conductivity function $K(\theta)$ (right) plotted for a homogeneous sand and a homogeneous silt. The dashed lines have been calculated using the Mualem-Brooks-Corey parametrization, the solid lines are based on the equivalent simplified Mualem-van Genuchten formulation. The parameters have been taken from *Roth* (2012).

and its inverse formulation

$$h_m(\Theta) = -\frac{1}{\alpha}\left[\Theta^{\frac{n}{1-n}} - 1\right]^{1/n}, \tag{3.20}$$

which has found the most widespread use in literature. The correct choice of a suitable parameterization may depend on the specific application. For example, the van Genuchten formulations have certain advantages for numerical simulations due to their differentiability. However, as has for example been shown by *Dagenbach et al.* (2012), the simplified van Genuchten parameterization is not necessarily suitable for describing the capillary fringe response in a sandy material to a Ground-Penetrating Radar signal. In this case either a Brooks-Corey type model or an equivalently formulated full van Genuchten parameterization has to be used. For more discussion on the different advantages and drawbacks of the different formulations, refer to *Dagenbach* (2012) or *Roth* (2012).

Far from the capillary fringe ($h_m \ll h_0$), the material models can be converted between each other via

$$\alpha = \frac{1}{h_0} \tag{3.21}$$

and

$$\lambda = n \cdot m = n - 1 \tag{3.22}$$

with exploits $m = 1 - 1/n$.

Hydraulic conductivity function

Similarly, the hydraulic conductivity function $K(\theta)$ will depend strongly on the pore geometry. This can be expressed by the model of *Mualem* (1976), which introduces a few additional parameters:

$$K(\Theta) = K_s \Theta^{\tau} \left[\frac{\int_0^{\Theta} h_m(\vartheta)^{-1} \, d\vartheta}{\int_0^{1} h_m(\vartheta)^{-1} \, d\vartheta} \right]^2 . \tag{3.23}$$

Here, K_s is the hydraulic conductivity at saturation, while the term Θ^{τ} is a measure for the tortuosity of the porous medium. In general, τ is simply treated as an additional fit parameter. Under most conditions a value of $\tau = 0.5$ is usually employed.

Inserting equation 3.15 into equation 3.23 yields the Mualem-Brooks-Corey model for the hydraulic conductivity function:

$$K(\Theta) = K_0 \Theta^{\tau+2+2/\lambda}. \tag{3.24}$$

Similarly, by inserting equation 3.20 into equation 3.23 and heeding the formal condition $0 < m < 1$, the corresponding Mualem-van Genuchten model is obtained with

$$K(\Theta) = K_s \Theta^{\tau} \left[1 - \left[1 - \Theta^{\frac{1}{m}} \right]^m \right]^2 . \tag{3.25}$$

3.4.2 Concluding remarks

In summary, these considerations leave us with a set of either six Mualem-Brooks-Corey parameters $\{\theta_s, \theta_r, h_0, \lambda, K_s, \tau\}$ or seven Mualem-van Genuchten parameters $\{\theta_s, \theta_r, \alpha, n, m, K_s, \tau\}$ which also get reduced to six for the simplified formulation. These parameters describe the physical properties of the considered medium and allow the description of soil water dynamics in the framework of the Richards equation as formulated above.
An overview of both relationships calculated for two different kinds of materials can be found in figure 3.4. The two most important results for our purposes which can be seen in these diagrams are (i) in a fine-grained silty material, the transition zone can be expected to be much wider than in a comparatively coarse grained sand, and (ii) the corresponding hydraulic conductivity functions may vary over several orders of magnitude with water content, most prominently for low water contents.

4 Electromagnetics

4.1 Electromagnetic Wave Propagation in Matter

4.1.1 Maxwell's Equations and Preliminary Assumptions

The relevant Maxwell's equations to study electromagnetic wave propagation are

$$\nabla \times \mathbf{H}(\mathbf{r},t) = \mathbf{J}_{\text{ext}}(\mathbf{r},t) + \frac{\partial}{\partial t}\mathbf{D}(\mathbf{r},t) \tag{4.1}$$

$$\nabla \times \mathbf{E}(\mathbf{r},t) = -\mu_0 \frac{\partial}{\partial t}\mathbf{H}(\mathbf{r},t) \quad . \tag{4.2}$$

[$\mathbf{E}$ - electrical field, $\mathbf{D}$ - displacement current, $\mathbf{H}$ - magnetic field]

[$\mathbf{J}_{\text{ext}}$ - external current density, μ_0 - vacuum permeability ($4\pi\times10^{-7}\text{N/A}^2$)]

Here, the equations are given for non-magnetic matter, because the most materials related to the experiments in this practical course are not magnetizable. Therefore, the relative magnetic permeability is set to 1. This is only violated, when soils with a non-negligible iron content are studied.

Furthermore, in equation 4.1 an external current density is mentioned. It is the source of the electromagnetic waves and therefore represents the antenna in the system.

4.1.2 The Electrical Conductivity

The electric conductivity results, when an incoming electric field leads to a movement of unbounded charge carriers. For its description, one can start with the equation of motion according to *Drude* (1900)

$$\frac{\partial^2}{\partial t^2}\mathbf{s}(\mathbf{r},t) + f\,\frac{\partial}{\partial t}\mathbf{s}(\mathbf{r},t) = \frac{q}{m}\,\mathbf{E}(\mathbf{r},t) \quad . \tag{4.3}$$

[$\mathbf{s}$ - elongation of particles from an initial position, f -damping term due to friction / collisions]

[m - mass of the particles, q - charge of the particles]

The movement of all particles with a particle density n leads to a resulting current density $\mathbf{J}$, which is given as

$$\mathbf{J}(\mathbf{r},t) = -n\,q\,\partial_t \mathbf{s}(\mathbf{r},t) \quad . \tag{4.4}$$

Substituting this into equation 4.3, this results

$$\partial_t \mathbf{J}(\mathbf{r},t) + f\,\mathbf{J}(\mathbf{r},t) = \frac{q^2\,n}{m}\,\mathbf{E}(\mathbf{r},t) \quad . \tag{4.5}$$

After a Fourier-transformation, rearranging the equation and employing Ohms Law $\mathbf{J}(\mathbf{r},\omega) = \sigma(\omega)\,\mathbf{E}(\mathbf{r},\omega)$, we obtain

$$\sigma(\omega) = \frac{q^2\,n}{(f - \mathtt{i}\,\omega)\,m} \tag{4.6}$$

[σ - electrical conductivity.]

Important: The electric conductivity is an effect of unbounded charge carriers and is in general a complex function of frequency. As can be seen in equations 4.17 and 4.18 attenuation of electromagnetic waves partly goes back to the real part of $\sigma(\omega)$ which itself depends on the damping factor f (You can see this by reformulating equation 4.6). Hence one can say that the damping of the movement of free charge carriers partly causes the attenuation; a fact that is quite intuitive. When using microwaves - as we do here - the damping term g is found to be dominating in equation 4.6. Then, the electric conductivity function reduces to the direct current electric conductivity $\sigma_{\mathrm{dc}} = \frac{q^2\,n}{f\,m}$.

4.1.3 The Dielectric Permittivity

The influence of dielectric material properties is introduced in the displacement current $\mathbf{D}$. Here, the idea is that an incoming oscillating electric field can lead to a polarization in the medium. This can be expressed as

$$\mathbf{D}(\mathbf{r},t) = \varepsilon_0\,\mathbf{E}(\mathbf{r},t) + \mathbf{P}(\mathbf{r},t) \quad . \tag{4.7}$$

[$\mathbf{P}$ - polarization, ε_0 - vacuum permittivity ($8.854...\times10^{-12}\mathrm{A^2s^4/kg\ m^3}$)]

This polarization results from displaced charges due to the electric fields[1]. Furthermore, the response due to the polarization induced by an incoming electric field is assumed to be linear, which is only violated in the research field of high energy laser physics. This response of the polarization need not to be instantaneous and it can have an aftereffect, which leads to a general description given as

$$\mathbf{P}(\mathbf{r},t) = \int_{-\infty}^{t} R(\mathbf{r},t-t')\,\mathbf{E}(\mathbf{r},t')\,dt' \quad , \tag{4.8}$$

which is a convolution of a response function R and the electric field. This response function describes how the medium reacts, when a single and very sharp electric field excitation (delta-excitation) occurs.

[1] A polarization can also be induced by the magnetic field. In the scope of this work, this will be neglected.

This expression leads to a simple product in the frequency domain, which yields

$$\mathbf{P}(\mathbf{r},\omega) = \chi(\mathbf{r},\omega)\ \mathbf{E}(\mathbf{r},\omega) \quad , \tag{4.9}$$

[χ - electric susceptibility, ω - angular frequency (ω=2$\pi\nu$), ν - physical frequency]

where χ represents the Fourier transformation of the response function R. Then, equation 4.7 leads in the frequency domain with equation 4.9 to

$$\mathbf{D}(\mathbf{r},\omega) = \varepsilon_0 \left(1 + \chi(\mathbf{r},\omega)\right) \mathbf{E}(\mathbf{r},\omega) = \varepsilon_0\ \varepsilon^*(\mathbf{r},\omega)\ \mathbf{E}(\mathbf{r},\omega) \quad . \tag{4.10}$$

Here, $\varepsilon^*(\mathbf{r},\omega) := 1 + \chi(\mathbf{r},\omega)$ is defined as the relative dielectric permittivity[2] of the medium.

Important: The relative dielectric permittivity is a quantity of the energy storage of the medium, due to a polarization of the medium. In the case that the response of the medium concerning an incoming electric field is instantaneously and without any aftereffect, than the relative permittivity is a constant. But in general it must be considered as a complex function

$$\varepsilon^*(\omega) \coloneqq \varepsilon^{*'}(\omega) - \mathtt{i}\ \varepsilon^{*''}(\omega) \tag{4.11}$$

depending on the frequency of the incoming electrical field. So, if each frequency component of an incoming electric signal leads to a different response of the medium, the outgoing signal is deformed. This is called dispersion.

One possible model to do derive a functional expression for $\varepsilon^*(\omega)$ is given by the Drude model (*Jackson* (2006), p. 358 ff.). This model assumes that the polarization of the medium is caused by atomic electrons which are located in a harmonic force field leading to an additional term $\omega_0^2\mathbf{s}(\mathbf{r},t)$ on the left hand of equation 4.3. This means that these electrons are assumed to be bound (by the harmonic force), which is the decisive difference to the derivation of the electrical conductivity in section 4.1.2. Exactly the bounding force leads to the appearance of *resoncance absorption*: In certain frequency ranges (absorption bands) around the resonance frequency ω_0 the entity $\varepsilon^{*''}(\omega)$ cannot be neglected and causes the attenuation of electromagnetic waves (equation 4.17).

Howsoever, the derivation of the functional expression for $\varepsilon^*(\omega)$ is of minor importance for this practical course. Hence, you are referred to the literature sources for a deeper insight.

Note: Electrical conductivity and the dielectric permittivity can be subsumed under a general relative permittivity via

$$\varepsilon(\omega) \coloneqq \frac{\sigma(\omega)}{\mathtt{i}\,\omega\,\varepsilon_0} + \varepsilon^*(\omega) \quad . \tag{4.12}$$

Obviously, this entity is in general a complex number with $\varepsilon(\omega) \coloneqq \varepsilon'(\omega) - \mathtt{i}\ \varepsilon''(\omega)$. (For simplicity reason, we keep the previously mentioned notation of the relative permittivity ε.)

[2] Normally, the notation ε_r can be found in the literature for the relative dielectric permittivity. Because, we always refer to this value in the scope of this manual, we neglect the index r.

4.1.4 Propagation of Electromagnetic Waves

An adequate approach solving equation 4.1 and 4.2 is the plane wave approach[3]. A single plane wave is mathematically described as

$$\mathbf{E}(\mathbf{r},t) = \mathbf{E}_0\, e^{\mathtt{i}(\omega\, t - \mathbf{k}\cdot\mathbf{r})} \quad . \tag{4.13}$$

[$\mathbf{E}_0$ - amplitude factor, $\mathbf{k}$ - propagation vector]

Here, the propagation vector gives mainly the propagation direction. With respect to Maxwell's equations, the dispersion relation

$$|\mathbf{k}|^2 = \omega^2\, \mu_0\, \varepsilon_0\, \varepsilon(\omega) = \frac{\omega^2}{c_0^2}\, \varepsilon(\omega) \tag{4.14}$$

[$c_0{=}(\varepsilon_0\, \mu_0)^{-1/2}$ - speed of light in vacuum ($c_0{\approx}0.3$m/ns)]

must be fulfilled. From this it is obvious that the length of the propagation vector depends on the frequency and cannot be chosen arbitrarily.

Propagation Velocity and Attenuation of Plane Waves

Attenuation of a single plane wave always appears if $\varepsilon''(\omega) \neq 0$. To understand this fact, we assume a plane wave propagating in the x-direction. Then, the phase of equation 4.13 can be rewritten with

$$k_x = \frac{\omega}{c_0}\sqrt{\varepsilon'(\omega) - \mathtt{i}\;\varepsilon''(\omega)} = \frac{\omega}{c_0}\sqrt{\varepsilon' - \mathtt{i}\;\varepsilon''} := \alpha - \mathtt{i}\beta \tag{4.15}$$

as

$$\mathtt{i}(\omega\, t - k_x x) = \mathtt{i}\big(\omega\, t - (\alpha - \mathtt{i}\beta)\, x\big) = -\beta\, x + \mathtt{i}(\omega\, t - \alpha\, x) \quad , \tag{4.16}$$

where α and β are defined as the real and imaginary part of the x-component of the propagation vector. Inserting this reformulation into equation 4.13, we can see that α is responsible for the propagation and β for the attenuation. One possible solution for α and β - which in general are functions of ε', ε'', and ω - is:

$$\alpha = \frac{\omega}{c_0}\sqrt{\frac{\varepsilon' + \sqrt{\varepsilon'^2 + \varepsilon''^2}}{2}} \text{ and } \beta = \frac{\omega}{c_0}\sqrt{\frac{-\varepsilon' + \sqrt{\varepsilon'^2 + \varepsilon''^2}}{2}}. \tag{4.17}$$

[3] Mathematically, this means that two plane waves propagating in opposite directions (linearly independent!) are a fundamental solution of the Maxwell equations for a given frequency. And because of the linearity of Maxwell's equations, any linear combination of plane waves with different frequencies obviously is a solution as well; Hence a big function space is covered by this, including wavelets (section 4.3.2). Thinking in the opposite direction, it also means that any observed electromagnetic field (which by definition is a solution to Maxwell's equations) can be represented by a linear combination of plane waves. A fact that is expressed by the often applied Fourier Transform or frequency decomposition. This all enhances the importance of plane waves and explains why it is typically sufficient to stay limited to plane waves in solving electrodynamic problems.

Important: The velocity and the attenuation of a plane wave are functions of both real and imaginary part of the relative permittivity. Generally, they depend on the frequency, meaning that each frequency component of an initial electromagnetic wave front is affected differently. This effect is called *dispersion of a wave front*.

Assuming that the relative permittivity has only a small imaginary part, which is only influenced by the electric conductivity, then the plane wave propagation in x-direction in the medium can be described as

$$\mathbf{E}(x,t) = \mathbf{E}_0 \exp\left\{-\sigma(\omega), x\right\} \exp\left\{\mathtt{i}\,\omega\left(t - \frac{\sqrt{\varepsilon'}}{c_0}\,x\right)\right\} \quad . \tag{4.18}$$

Note: The terms *attenuation* and *absorption* are not consistently used in literature. Sometimes both expressions are used equivalently what increases confusion and is obviously redundant. Thus, we want to distinguish between the two processes here, according to the following definition: Absorption is only related to the processes included in $\varepsilon''(\omega)$: Resonance absorption and the damping of free charge carrier movement. Attenuation says something about the electromagnetic wave amplitude: Inserting the equation 4.16 in 4.13, we directly see that the plane wave is attenuated by the factor $\exp\{-\beta x\}$ (β is sometimes also called attenuation coefficient). Hence, in general attenuation includes imaginary *and* real parts of ε. Therefore, absorption is included as well as scattering and other effects. However, it is interesting to notice that $\varepsilon'' \neq 0$ ($\rightarrow$ absorption) is still a necessary condition for $\beta \neq 0$ ($\rightarrow$ attenuation). This might be one reason for the given confusion on the two terms.

4.2 Guided Waves - Transmission Line Theory

Equations 4.1 and 4.2 are the general expressions of Maxwell's theory, they can be easily applied to study the propagation of freely propagating waves. If we focus on guided waves in conductors, then the geometry plays a significant role in the wave propagation.

The theory of the propagation of guided waves in electromagnetism is subsumed in the transmission line theory. Here, the relevant observable quantities are the voltage V and the current I. The wave equation in frequency domain for both quantities propagating only in one dimension (x-direction) are

$$\partial_x^2 V(x) + \omega^2\, LC\, V(x) = 0 \tag{4.19}$$

$$\partial_x^2 I(x) + \omega^2\, LC\, I(x) = 0 \quad . \tag{4.20}$$

[L - inductance, C - conductance]

Using a similar approach as equation 4.13 for the voltage or the current, one can obtain a propagation velocity

$$v = \frac{1}{\sqrt{LC}} = F\,\frac{1}{\sqrt{\mu_o\,\varepsilon_0\,\varepsilon'}} = F\,\frac{c_0}{\sqrt{\varepsilon'}} \quad . \tag{4.21}$$

Here, a form-factor F is introduced in order to account for the fact, that the velocity is influenced by the geometry of the system. In this practical course, the TDR probes are designed in a way, that F can be assumed as 1.

4.3 Measuring Material Properties with Electromagnetic Waves

When applying electromagnetic waves to measure material properties, one could basically use two different techniques: (i) transmission or (ii) reflection. For both methods, one can either evaluate the travel time or the electromagnetic wave amplitude to obtain information about the material, in which the wave was propagating.

Because in this practical course, we will focus on reflection measurements, a short overview of the concepts used for this measurement type will be given.

4.3.1 The Reflection Coefficient

For freely propagating waves a reflection always occurs, when the material properties are changing. Assuming the magnetic permeability to be constant and a perpendicular incidence, the reflection coefficient is given as

$$r = \frac{\sqrt{\varepsilon_1} - \sqrt{\varepsilon_2}}{\sqrt{\varepsilon_1} + \sqrt{\varepsilon_2}} \quad . \tag{4.22}$$

[ε_1 - relative permittivity of the upper layer, ε_2 - relative permittivity of the lower layer]

This is a special formulation of Fresnel's equation for the reflection of electromagnetic waves. The Reflection coefficient is the amplitude ratio of the incident to the reflected wave. Thus, its sign indicates a possible phase shift: if $r < 0$ a phase factor $e^{i\pi}$ is given. In case of a wavelet (next section), this means that the wavelet is flipped such that positive amplitudes get negative and vice versa.

Note: This equation is not generally valid for guided waves. Here, a change in the geometry can also lead to a reflection, although the material properties remain constant.

4.3.2 Wavelet Concept

In the field of GPR and TDR applications, it is assumed that an electromagnetic pulse with a finite duration in time and a specific shape is emitted. This pulse propagates in the adjacent medium and it is either directly transmitted to the receiver or it reaches the receiver after one or several reflections. The sum of all incoming pulses is the measured signal.

This pulse can be called wavelet and therefore, the measured signal can be considered as a superposition of wavelets, where each wavelet travels along a different propagation path.

In a lot of cases, the measured signal cannot be simply decomposed. For TDR applications this is mainly due to the dispersion of the initial pulse. For GPR applications this results from the superposition of different wavelets. Hence, in most applications either of TDR or GPR, one is trying to identify significant wavelet features. Assuming them to stay almost undisturbed, one can describe the propagation of these features with the ray approach.

4.4 The Relative Dielectric Permittivity of Soils

Soils can be considered as a three phase medium consisting of the soil matrix, air and water. Therefore, one has to study the permittivity of each constituent and then of the mixture. As the permittivity is determined by measuring the wave propagation velocity, only the real part ε' can be measured.

Because the relative permittivity of air ($\varepsilon'_{\text{air}} \approx 1$) and the soil matrix ($\varepsilon'_{\text{matrix}} \approx 4-5$) can be considered as constant values in the frequency range of TDR and GPR, we will focus on the relative permittivity of water and of the mixture.

4.4.1 The Relative Permittivity of Water

Each water molecule can be considered as a dipole, which can be orientated according to an incoming electromagnetic field. This orientation of the molecules depends on the frequency of the incoming field. Hence three cases have to be distinguished.

- If the frequency is too high, the molecules cannot follow and thus, they cannot store electromagnetic energy. This results in a smaller value of the relative permittivity of water.
- If the frequency is slower than the time for the orientation of each molecule, then the polarization of the water can reach its maximum, which results in the highest number of the relative permittivity value.
- For the frequency between these sketched limits, the molecules can follow partially the alternating electromagnetic fields. Therefore, electromagnetic energy is needed to orientate the molecules. This energy is either re-emitted or transformed into thermal energy. This phenomenon is called relaxation process, because the reemission is not instantaneously. Furthermore, it is coupled with absorption of the electromagnetic waves. The frequency at which the most energy is absorbed is called relaxation frequency.

In addition, the capability for the polarization for the water molecules as well as the relaxation process and the absorption of electromagnetic energy is a function of temperature. That is because the Brownian motion, which depends on the temperature, counteracts the orientation of the motions.

Note: For frequencies below 1 GHz, the dielectric permittivity of water can be assumed to be frequency independent and the imaginary part can be neglected (*Gerhards* (2008), p. 17). Including temperature the ε' can be described as a function of temperature according to *Kaatze* (1989) as

$$\log_{10} \varepsilon'_{\text{water}} = 1.94404 - 1.991 \cdot 10^{-3}\,\text{K}^{-1} \cdot (T - 273.15\,\text{K}) \quad . \tag{4.23}$$

[T - temperature in K (Kelvin)]

5 Petrophysical Relationship

Over the last decades, a multitude of different models have been proposed for calculating the composite permittivity of soils ε'_c, ranging from purely empirical relationships to more physically inspired mixing models.

In general, the calculation of ε'_c is a non-trivial issue. For example, if at least one constituent exhibits a relaxation behavior in the frequency window of interest, then the interaction of all constituents can change this relaxation process or even lead to a multi-relaxation phenomenon, e.g., due to different molecule interactions as a function of the distance to surfaces.

If we assume however, that none of the constituents undergoes relaxation, a simple mixing formula can be applied. Such a model expresses ε'_c as a weighted average of the permittivity of all the constituents in the soil. One general formulation has been called the 'Lichteneker-Rother' equation (e.g., *Brovelli and Cassiani* (2008)) given by:

$$\varepsilon_c^\alpha = \sum_{i=1}^{n} \theta_i \varepsilon_i^\alpha \quad , \tag{5.1}$$

where n denotes the number of constituent phases and the exponent α is a fitting parameter ($-1 \leq \alpha \leq 1$, depending on the alignment of microscopic structures of the considered composite material with respect to the passing electromagnetic wave). For random alignment of microscopic structures, $\alpha = 0.5$, leading to the so-called Complex Refractive Index Model ('CRIM', e.g., *Birchak et al.* (1974), or *Roth et al.* (1990)). Explicitly writing out the sum in equation 5.1 for the three-phase case of soil matrix, air and water, the composite dielectric permittivity ε'_c can then expressed as

$$\sqrt{\varepsilon'_c} = \theta \sqrt{\varepsilon'_{\text{water}}} + (\phi - \theta) \sqrt{\varepsilon'_{\text{air}}} + (1 - \phi) \sqrt{\varepsilon'_{\text{matrix}}} \quad , \tag{5.2}$$

[θ - volumetric water content, ϕ - porosity]

Rearranging this equation, one can deduce a formula to determine the volumetric water content via

$$\begin{aligned} \theta &= \frac{\sqrt{\varepsilon'_c} - \sqrt{\varepsilon'_{\text{matrix}}} - \phi \left(\sqrt{\varepsilon'_{\text{air}}} - \sqrt{\varepsilon'_{\text{matrix}}} \right)}{\sqrt{\varepsilon'_{\text{water}}} - \sqrt{\varepsilon'_{\text{air}}}} \\ &= \frac{1}{\sqrt{\varepsilon'_{\text{water}}} - 1} \sqrt{\varepsilon'_c} - \frac{(1 - \phi) \sqrt{\varepsilon'_{\text{matrix}}} + \phi}{\sqrt{\varepsilon'_{\text{water}}} - 1} \quad , \end{aligned} \tag{5.3}$$

which is essentially a linear relationship as a function of the composite dielectric permittivity. Such a functional relationship between a parameter which can be directly measured with geophysical methods (here the composite dielectric permittivity ε'_c) and a secondary quantity of interest (here the hydrologic quantity of soil water content θ) is commonly called a **petrophysical relationship**.
In our case, measuring the composite relative permittivity allows to determine the water content in the soil, provided we have additional knowledge or at least reasonable assumptions about the porosity ϕ, the relative permittivity of the soil matrix $\varepsilon'_{\text{matrix}}$ as well as the temperature, which is needed for calculating the permittivity of water $\varepsilon'_{\text{water}}$ as described in the previous chapter.

6 Time Domain Reflectometry

In soil science, time domain reflectometry (TDR) is a state-of-the-art method to measure volumetric water content and electrical conductivity of soils. The measurement principle is based on the analysis of the propagation velocity of guided electromagnetic waves along a TDR probe through the ground. It allows to determine the dielectric properties of the medium which are closely related to water content and electrical conductivity. For interested students, a comprehensive review of the TDR measurement technique is given by *Robinson et al.* (2003).

6.1 Measurement Principle

A schematic description of a TDR measurement system is shown in figure 6.1. It consists of a TDR device which is composed of a signal generator and a sampling unit, and a TDR probe that is connected to the TDR device via a coaxial cable. The system applied in this practical course is controlled by a computer.

The measurement principle is based on the measurement of the propagation velocity of a step voltage pulse along a TDR probe through the ground. The probe is installed such, that the metal rods are completely surrounded by the soil material. In this experiment, we apply 3-rod TDR probes where the probe rods are arranged in a horizontal plane with a constant separation between the rods. In principle, the probe rods can be regarded as an elongation of the coaxial cable where the middle rod is the inner conductor and the outer rods represent the outer conductor of the cable. The TDR device generates short electromagnetic pulses (frequency range: 20 kHz to 1.5 GHz) which propagate along the coaxial cable and further along the rods of the TDR probe. At positions where erratic changes in relative permittivity occur, part of the electromagnetic energy is reflected. This is why TDR was initially developed for detecting failures along transmission line cables - TDR devices are also known as “cable testers”. The application in soil science is a modification of this technique. At the head of the TDR probe, part of the electromagnetic energy is reflected due to the impedance jump between the cable and probe head material. The remaining fraction of the signal propagates through the soil along the metal rods which serve as a wave guide. At positions where the dielectric properties of the soil change erratically, the signal is again partially reflected. In soils with low electrical conductivity, the remaining part of the electromagnetic energy is finally reflected at the end of the probe rods.

The temporal development of the voltage of the reflected TDR signal is recorded by the

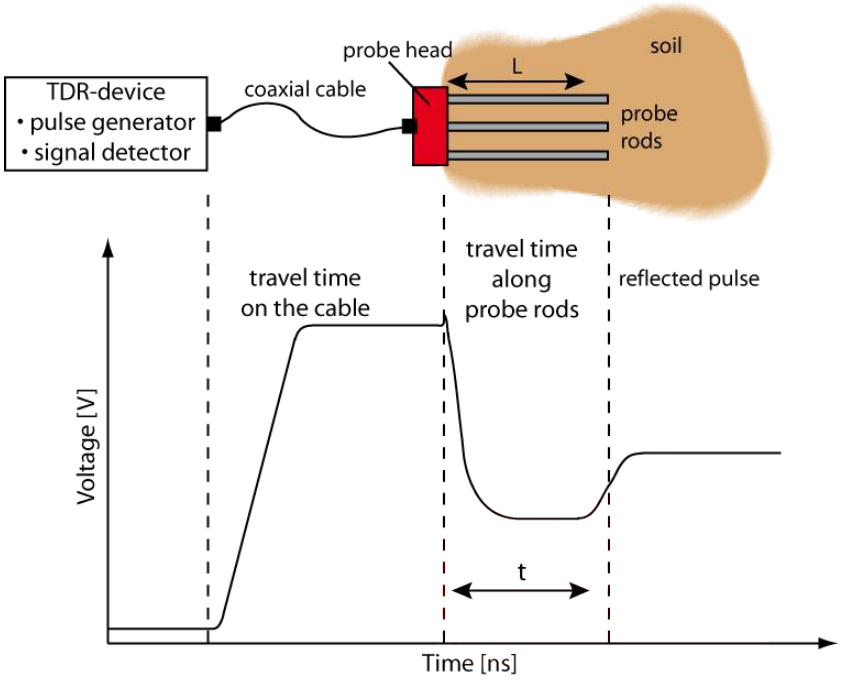

Figure 6.1: Measurement principle of a TDR probe and example signal

signal detector of the TDR device. Figure 6.1 shows a characteristic voltage-time diagram as obtained in a TDR measurement. From the signal response we can deduce the electrical properties of the material through which the electromagnetic pulse propagates.

6.2 Evaluation of the TDR Signal

For the determination of the travel time of the electromagnetic signal along the TDR rods through the soil we use the two significant reflections which occur in the head and at the end of the rods of the TDR probe. From these two characteristic points we can deduce the two-way travel time t_{rod} of the electromagnetic signal through the soil: forth to the end of the probe and back to the probe head. With that one obtains the composite relative permittivity of the material which surrounds the probe rods

$$\varepsilon_c' = \left(\frac{c t_{rod}}{2L} \right)^2 , \tag{6.1}$$

where L is the length of the TDR probe rods. The volumetric soil water content is determined from the measured relative permittivity using the CRIM formula (equation 5.3).

The reflection from the probe head is independent of the material between the probe rods an hence occurs always at the same travel time and serves as a reference in the travel

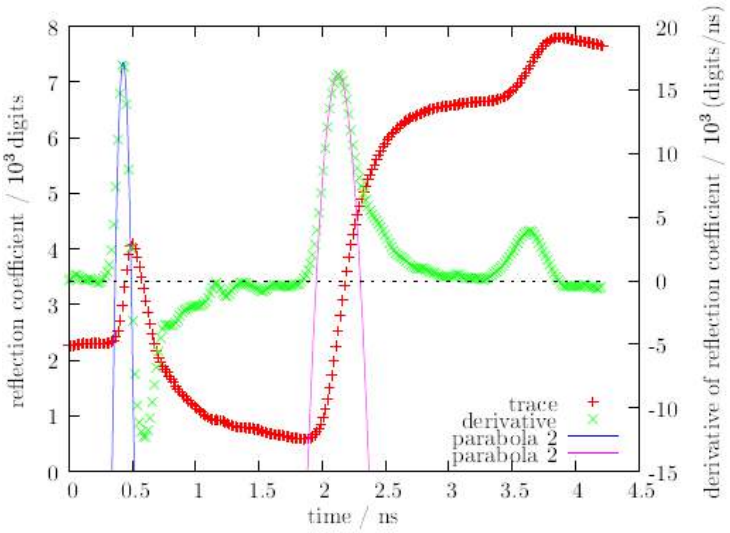

Figure 6.2: Travel time determination from the TDR signal

time calculation. The travel time of the reflection from the rod ends depends on the propagation velocity of the electromagnetic wave through the soil. The difference of these two reflection points determines the travel time of the electromagnetic signal forth and back through the soil.

The travel time composes of the travel time through the probe head and along the probe rods:

$$t_{probe} = t_{head} + t_{rods}. \tag{6.2}$$

For an accurate determination of the soil's relative permittivity the TDR probes first have to be calibrated in media with known propagation velocities. In our case the calibration is done by conducting TDR measurements in water and air and correcting for the travel time in the probe head.

Determination of the travel time of the electromagnetic signal is done by using the derivative of the TDR signal and taking the largest values of the derivative occurring at the impedance jump in the probe head and at the end of the rod as reference points (see figure 6.2).

6.3 Electrical Conductivity

A comprehensive description for measuring electrical conductivity of soils with TDR is given by *Heimovaara et al.* (1995). The direct current electric conductivity σ_{dc} of the soil can be determined from the amplitude of the reflected TDR signal:

$$\sigma_{\mathrm{dc}} = \frac{K}{Z}\frac{1 - R_\infty}{1 + R_\infty}. \tag{6.3}$$

where K is a constant which is determined by the probe geometry, Z is the impedance of the cable (50 Ω), and R_∞ is the reflection coefficient at very long travel times where

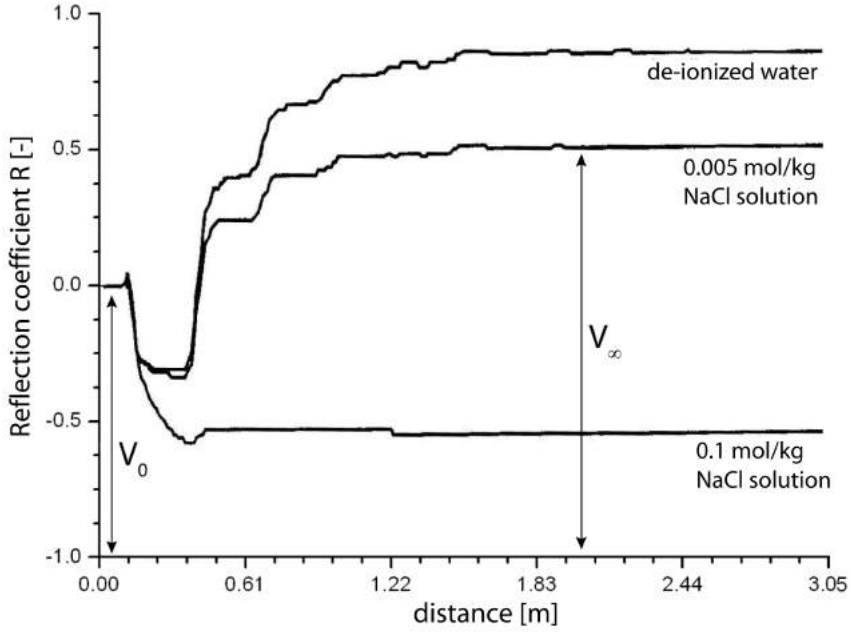

Figure 6.3: TDR signals for determination of electrical conductivity. Note, that the TDR100 device used in the practical course directly translates measured voltages into reflection coefficients.

no further reflections of the signal occur. At this point the reflection coefficient can be determined by

$$R_\infty = \frac{V_\infty - V_0}{V_0} \tag{6.4}$$

where V_∞ and V_0 are the signal amplitudes as shown in Figure 6.3.

The probe geometry constant K can be determined by measuring signals in solutions with known electrical conductivity $\sigma_{\mathrm{dc,T}}$ (at T °C). Alternatively, K can be determined by

$$K = \left(\frac{\varepsilon_0 \varepsilon'}{L}\right) Z_0 \tag{6.5}$$

where ε_0 is the electrical field constant, ε' is the relative permittivity in free space, L is the probe rod length [m] and Z_0 is the probe capacity. Z_0 can be determined via a reference measurement in non-conductive material, as e.g. de-ionized water using

$$Z_0 = Z\varepsilon'_{ref}\left(\frac{1+R_0}{1-R_0}\right) \tag{6.6}$$

where ε'_{ref} is the relative permittivity of the non-conductive medium.

6.4 Measurement Volume

The measurement volume of a TDR probe is the volume of soil which has an influence on the measured TDR signal.

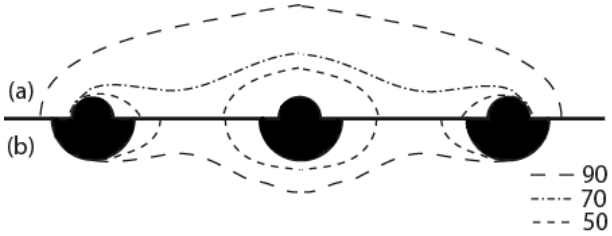

Figure 6.4: Volume fractions of the total sampling volume (a) rod distance : rod diameter = 10 (b) rod distance : rod diameter = 5

The sensitivity of the TDR probe decreases exponentially perpendicular to the rod axes. The volume fractions shown in figure 6.4 are determined by the probe geometry and are independent of the permittivity of the surrounding material. The measurement volume is primarily determined by the diameter and the distance between the probe rods: an increase in rod diameter leads to a smaller measurement volume; a larger rod distance causes a stronger attenuation of the high-frequency components of the TDR signal and hence a smaller measurement volume.

6.5 Concluding Remarks

TDR probes can be installed vertically and horizontally in the soil. This way, one can investigate the complete profile down to a depth of a few meters. As discussed in section 6.4 the effective measurement volume of a TDR probe is relatively small. Hence, water contents determined from this method only represent local point measurements. For a spatial analysis of soil water content at the field scale a huge number of measurements is required. Furthermore, one has to apply adequate interpolation techniques in order to obtain meaningful spatial information about water content distribution. Nevertheless, TDR is still a state-of-the-art technique in classical soil physics.

In order to obtain a good TDR measurement it is necessary to establish a good contact between the soil and the probe rods and to avoid air gaps during installation.

In this practical course we exclusively measure average soil moisture content along the probe rods even if the water content may be changing. Currently inverse techniques are being developed in soil physics which allow to model the TDR signal and estimate spatial changes in soil moisture content along the TDR probe. However, these techniques are computationally intensive and still in a development state and cannot be applied in the framework of this practical course.

7 Ground Penetrating Radar

Ground penetrating radar (GPR, RADAR = RAdio Detection And Ranging) is a state-of-the-art geophysical measurement technique which can be applied to explore near-surface underground structures. The measurement principle is based on the transmittance of high-frequency electromagnetic pulses into the ground. The travel time of the emitted pulses is subsequently recorded by a receiving antenna.

7.1 Measurement Principle

Standard ground penetrating radar systems consist of a transmitting and a receiving antenna. High-frequency (range: 50 MHz to 1 GHz) electromagnetic pulses are emitted into the ground by the transmitting antenna. The radar wavelet propagates through the soil while the velocity of the wavelet depends on the dielectric properties of the ground. At interfaces, e.g., boundaries of different soil layers or distinct objects, where the dielectric properties of the different media change erratically, the electromagnetic wave is partially reflected. The travel time and amplitude of the wavelet is recorded by the receiving antenna.

In contrast to the TDR technique which has been discussed in the previous chapter, GPR operates with "free" waves. The travel time of the wavelet which is recorded by the receiving antenna depends on the path along which the wavelet propagates and the dielectric properties of the materials. Figure 7.2 shows travel path of various wave types through the soil which may occur in the presence of two layers with different relative permittivities.

The first wavelet which is detected by the receiving antennas the so-called air wave which propagates through the air between both antennas with the vacuum speed of light. The second wavelet which reaches the receiver is the so-called ground wave. It propagates also directly between the transmitter and the receiver along the air-soil interface and can be applied to infer the near-surface soil moisture content. Air- and ground wave are also known as "direct waves" which always occur, independent of soil structure.

In layered soils we can detect further, reflected and refracted wavelets. Reflections occur at interfaces between soil layers with different dielectric properties. If $\varepsilon'_1 > \varepsilon'_2$, a further type of wave, the so-called refracted wave originate which propagates parallel to the boundary of the second layer. In addition, combinations of these primary wave types shown in Figure 7.2 may occur in the radargram which are not discussed here.

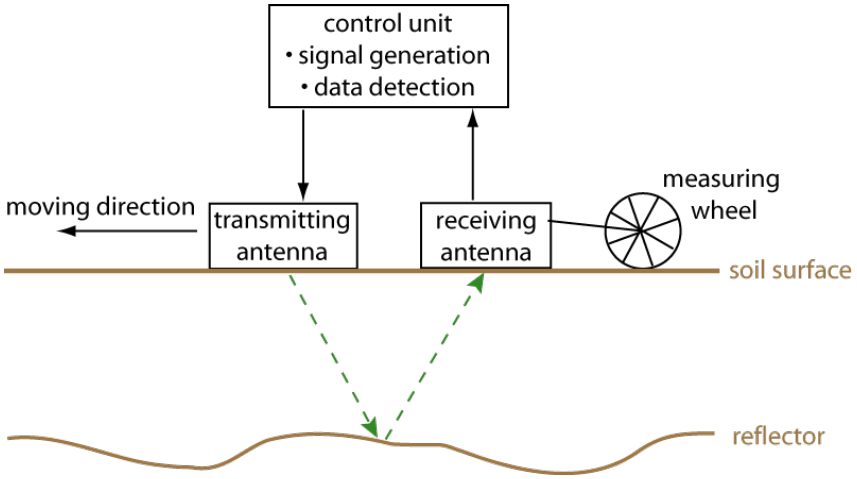

Figure 7.1: Ground penetrating radar measurement principle

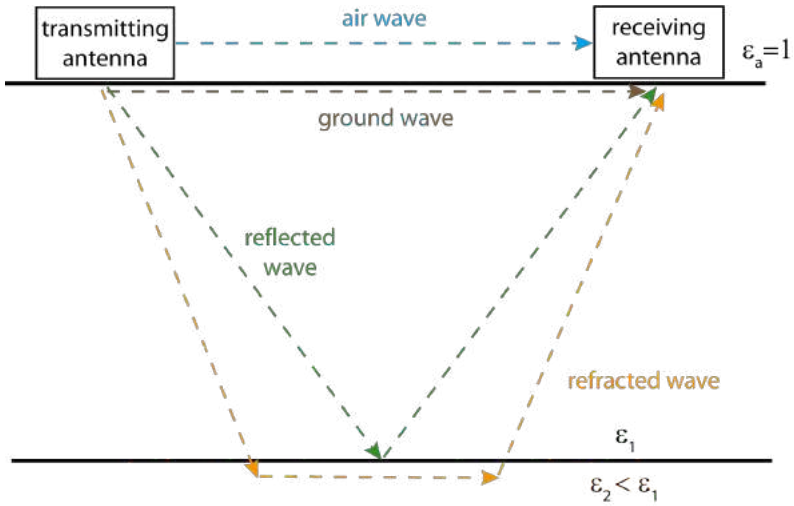

Figure 7.2: Travel paths of different GPR wave types in a two-layer soil with different relative permittivities.

The signals of the various emitted wavelets reach the receiving antenna at different times. Plotting the recorded amplitudes as a function of time results in a so-called "trace". Figure 7.3 shows a trace which consists of air wave, ground wave and reflected wave.

In a standard GPR measurement, the antennas are pulled along the survey track while traces are triggered at a fixed interval by a measurement wheel which is connected to the back of the antenna. This results in a series of traces which are finally displayed by the measurement software as a function of position and time in a so-called radargram.

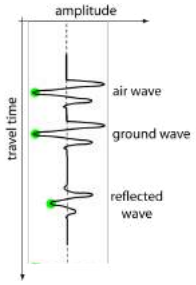

Figure 7.3: GPR trace. Note, that a wavelet always consists of a number of "wiggles" which are displayed in the radargram as a series of lines (e.g. red-blue-red)

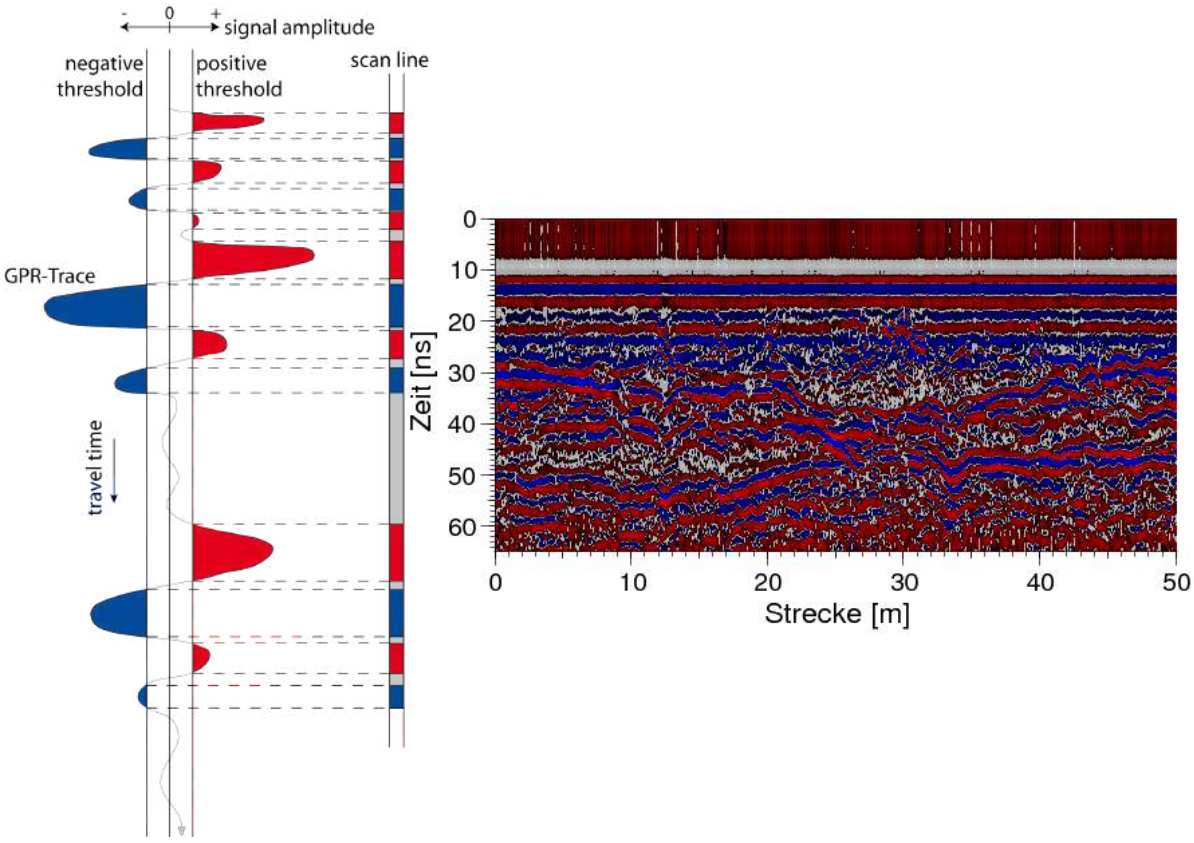

Figure 7.4: (a) Origin of a radargram. Amplitudes which excess a pre-defined positive or negative threshold are displayed in color. In this example negative amplitudes are shown in blue while positive amplitudes are displayed in red; modified after (*Reynolds*, 1997) (b) Example radargram.

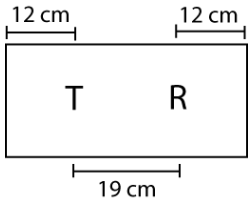

Figure 7.5: Construction and dimensions of an IDS antenna box (200 MHz)

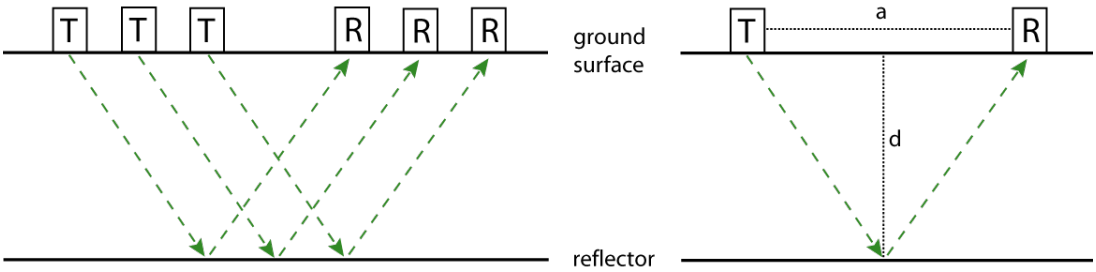

Figure 7.6: Common Offset

7.2 Measurement System

A GPR measurement system consists of a transmitter and a receiver antenna and a control unit (see Figure **??**). In the system applied in this practical course both antennas are placed in one box. The dimensions of these box are given in Figure 7.5.

The main part of the GPR system is the control unit which generates the GPR signal and also receives the signals after their passage through the ground. The complete system is computer controlled. The measurement wheel at the back of the antenna box measures the distance along the survey track and triggers the emittance of the electromagnetic pulses.

7.3 Measurement Setups

7.3.1 Common Offset (CO)

Common Offset is the simplest an most widespread GPR measurement technique. In this setup transmitter and receiver antennas are moved along the survey track while the distance between both antennas is kept constant throughout the whole survey. Electromagnetic pulses are emitted at equidistant intervals which are controlled by the survey wheel. With this measurement technique one can efficiently and fast obtain information about the near-surface underground structure.

From the measured travel time t of the reflected electromagnetic signal one can determine

the depth d of a horizontal reflector Figure 7.6

$$s = 2 \cdot \sqrt{d^2 + \left(\frac{a}{2}\right)^2} = \sqrt{4d^2 + a^2} \ , \tag{7.1}$$

where a is the distance between transmitting and receiving antenna. Assuming a homogeneous medium the travel time is determined by

$$t = \frac{s}{v} = \frac{\sqrt{4d^2 + a^2}}{\frac{c}{\sqrt{\varepsilon'}}}. \tag{7.2}$$

If the depth of the reflector is known, the relative permittivity can be determined which finally allows the calculation of the average volumetric water content of this layer via the CRIM formula (equation 5.3). However, usually the depth of the reflecting interface is not known. Hence, a CO measurement usually provides too less information for a thorough estimation of soil water content. At least it needs to be completed by independent information obtained from boreholes or soil profiles or by a so-called common-midpoint measurement which is described in the following section.

Multi Offset: Common Midpoint and Wide Angle Reflection and Refraction

In a common-midpoint measurement (CMP) transmitter and receiver are moved away from each other in equidistant steps (see Figure 7.7). At each position a trace is measured. This way, the reflected signal can be measured using a number of different angles. The resulting radargram displays the travel time as a function of the antenna separation (see Figure 7.8).

Since air and ground wave travel directly between the transmitting and receiving antenna, there is a linear relationship between the travel time t of each wave and the antenna separation a with the constant of proportionality $\frac{1}{v}$:

$$t = \frac{a}{v} \ , \tag{7.3}$$

with $v = c$ for the air wave and $v = \frac{c}{\sqrt{\varepsilon'}}$ for the ground wave. Due to their different velocities the slopes of both direct waves in the travel time diagram are different.

Consequently, the propagation velocity v of the GPR wave through the soil can be determined directly from the radargram by estimating the slope of the ground wave. Using (4.18) one obtains the average relative permittivity and with (5.3) also the average volumetric water content. Since the ground wave travels near the soil-air interface it covers that soil section which is for example important for plant growth. The air wave travel time is usually applied during data processing as reference for calculating absolute travel times.

From a CMP measurement one can determine the reflector depth below the midpoint between the transmitting and the receiving antenna: the relation between travel time t reflector depth d is given by Equation 7.1.

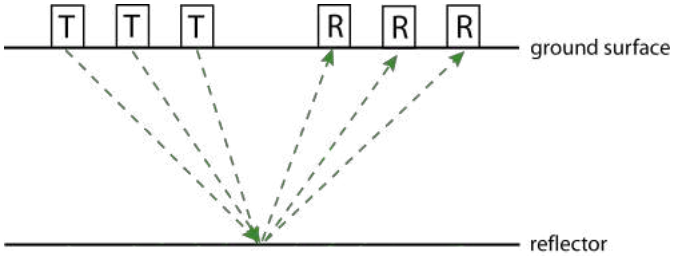

Figure 7.7: Common Midpoint

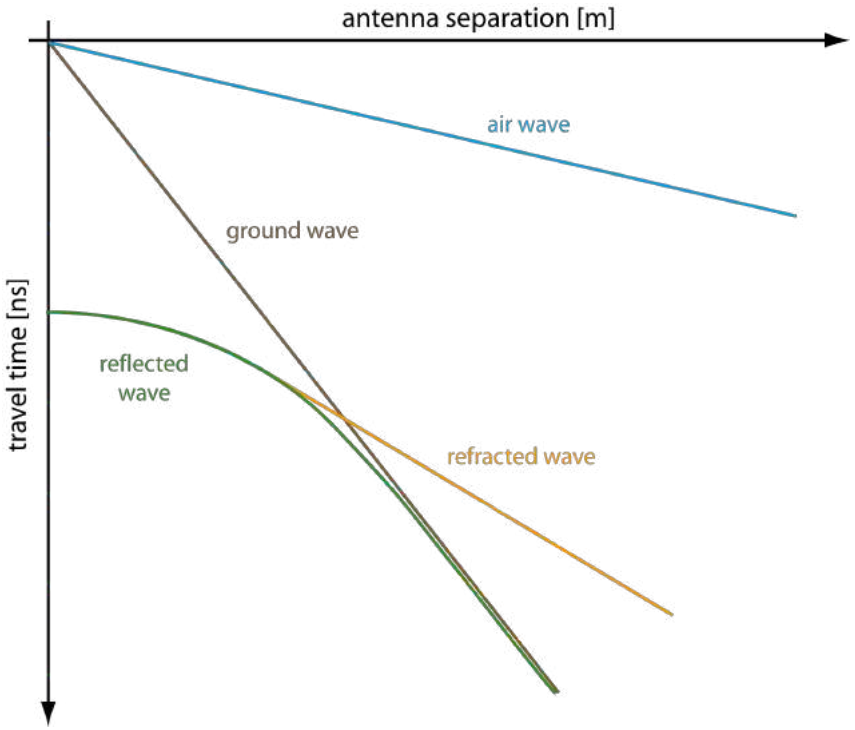

Figure 7.8: CMP-radargram

From the reflection hyperbolas displayed in the travel time diagram relative permittivity and reflector depth can be determined independently. Plotting the measured data in a t^2-a^2-diagram, leads to a linear relationship between t and a:

$$t^2 = \frac{1}{v^2}a^2 + \frac{4h^2}{v^2}. \tag{7.4}$$

The propagation velocity of the electromagnetic wave can now be directly determined from the slope of line. The depth of the reflector can be directly inferred from the intersection of the line with the y-axis.

In contrast to a CMP measurement, in a Wide Angle Reflection and Refraction (WARR) measurement (Figure 7.9) only the transmitting or receiving antenna is moved along the measurement line while the other antenna stays stationary.

In principle, a WARR measurement follows the same relationships concerning travel time as a CMP measurement. The difference is that the reflection point moves along the

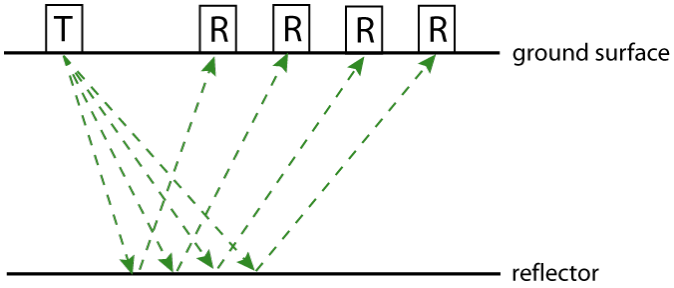

Figure 7.9: Wide Angle Reflection and Refraction

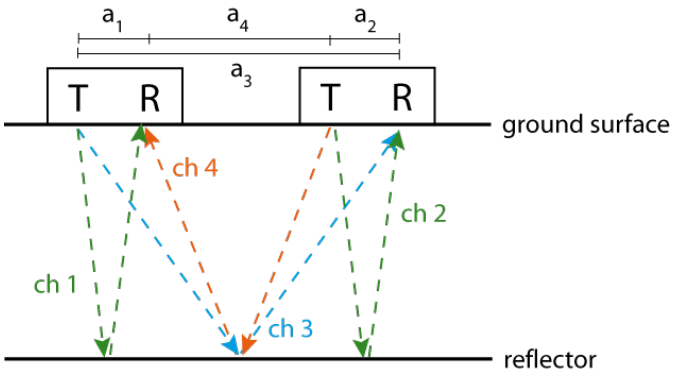

Figure 7.10: Antenna System

reflector. This is why a WARR measurement strictly is only applicable in the presence of horizontal or only slightly sloping reflectors and material properties are homogeneous.

In summary, CMP and WARR measurements provide more information than a CO measurement. The drawback of these techniques is the high measurement effort since both procedures only provide point information for a specific location. Hence, both methods are hardly applicable along long measurement lines.

7.3.2 Multi-channel GPR

In order to be able to conduct a measurement with acceptable effort and acquire almost as much information as in a series of CMP or WARR measurements, *Gerhards* (2008) developed a multi-channel GPR measurement technique. This new method combines the traditional CO and CMP measurement techniques. In this setup at least two standard GPR units, each consisting of a transmitting and a receiving antenna are coupled in a row at a fixed distance and are moved along the survey track (Figure 7.10). The multi-channel unit is able to acquire data from all available transmitter-receiver combinations. In the example given in Figure 7.10 this leads to four measurement channels which can be used to record common-offset radargrams simultaneously but with different antenna separations. The survey is almost as fast as a standard common-offset measurement with only one single antenna system.

In a setup build of two antenna systems the four available channels can, e.g., be combined as follows:

Channel 1 transmitter 1 combined with receiver 1 (T1R1)

Channel 2 transmitter 2 combined with receiver 2 (T2R2)

Channel 3 transmitter 1 combined with receiver 2 (T1R2)

Here, channels 1 and 2 use the standard common offset antenna separation $a_1 = a_2 =$ const. The antenna separations for channels 3 and 4 (a_3, a_4) can be selected by the operator (Figure 7.10).

The optimal antenna separation is

$$a_{opt} = \frac{2h}{\sqrt{\varepsilon' - 1}}. \tag{7.5}$$

If no information about the measurement site is available one usually uses the rule of thumb $a_{opt} = 0,2\ h$, where h is the desired penetration depth.

From a multi-channel GPR measurement it is possible to effectively estimate reflector depth h and relative permittivity ε' with minimal effort. The information can subsequently be used to determine the average volumetric soil moisture content θ using the CRIM formula (Equation 5.3). Here, at least two absolute travel times are required for one distinct measurement position.

$$h = \frac{1}{2}\sqrt{\frac{t_i^2 a_j^2 - t_j^2 a_i^2}{t_j^2 - t_i^2}} \tag{7.6}$$

$$\varepsilon = \frac{c^2 t_i^2}{4h^2 + a_i^2} \tag{7.7}$$

A multi-channel GPR measurement is kind of a moving mini-CMP measurement: The radargrams 1 and 2 (Figure 7.10) are shifted laterally such that the measurement points are consistent with those of channels 3 and 4. This way, one obtains three measurements at one single location with different antenna separations.

In order to obtain absolute values for relative permittivity and reflector depth, also absolute travel times are required which are initially not known from a radargram. Due to experimental difficulties, each radargram has an unknown offset which, however, can be determined from the theoretical travel time of the air wave t_{air} using

$$t_{air} = \frac{a}{c} = t - t_{off}. \tag{7.8}$$

Here, t_{off} is the unknown offset which has to be determined from the radargrams. It can be calculated from the travel time of the air wave at antenna separation $a = 0$. However,

since it is practically impossible to measure the travel time at this distance, one has to find a different way to retrieve this value. For the measurement we consider here, this offset can be determined from a calibration measurement as shown in figure **??** (*How?*). After performing the offset correction (equation 7.8) it is possible to quantitatively analyze the measured radargrams.

7.4 Energy Loss and Penetration Depth

As already mentioned in section 4.1.4, the electromagnetic signal is attenuated by different processes on its way through the soil. Figure 7.11 gives an overview of the different processes that lead to a reduction of signal strength.

The largest amount of energy loss results from damping of free charge carrier movement. Under the assumptions made for equation 4.18, the material dependent attenuation is induced by the direct current electric conductivity σ_{dc} of the investigated medium. Depending on the traveled distance x the amplitude E of the electromagnetic wave decreases exponential with respect to its starting value E_0:

$$E(x) = E_0 e^{-\beta x} \tag{7.9}$$

For the loss constant β one obtains after the above mentioned simplifications

$$\beta = \frac{\sigma_{\mathrm{dc}}}{2\, c_0\, \varepsilon_0\, \sqrt{\varepsilon'}}. \tag{7.10}$$

The higher σ_{dc} of the medium, the higher is the attenuation of the electromagnetic wave. In soils, electrical conductivity for example increases due to an increase in soil moisture content, clay content or amount of dissolved solutes in the soil solution.

The penetration depth of the electromagnetic wave

$$\delta = \frac{1}{\beta} \tag{7.11}$$

reduces with increasing electrical conductivity of the medium. For salt water the penetration depth is only $\delta_{saltwater} = 1$ cm.

In addition, so-called spherical losses occur which are caused by the field geometry of the measurement. The energy density is reduced due to geometrical spreading with the inverse of the square of the traveled path.

Scattering and diffraction of the electromagnetic energy at objects whose dimensions are in the same order of magnitude as the wavelength of the incident electromagnetic wave (Mie scattering) lead to a redirection of the energy which then cannot be registered any more by the receiving antenna.

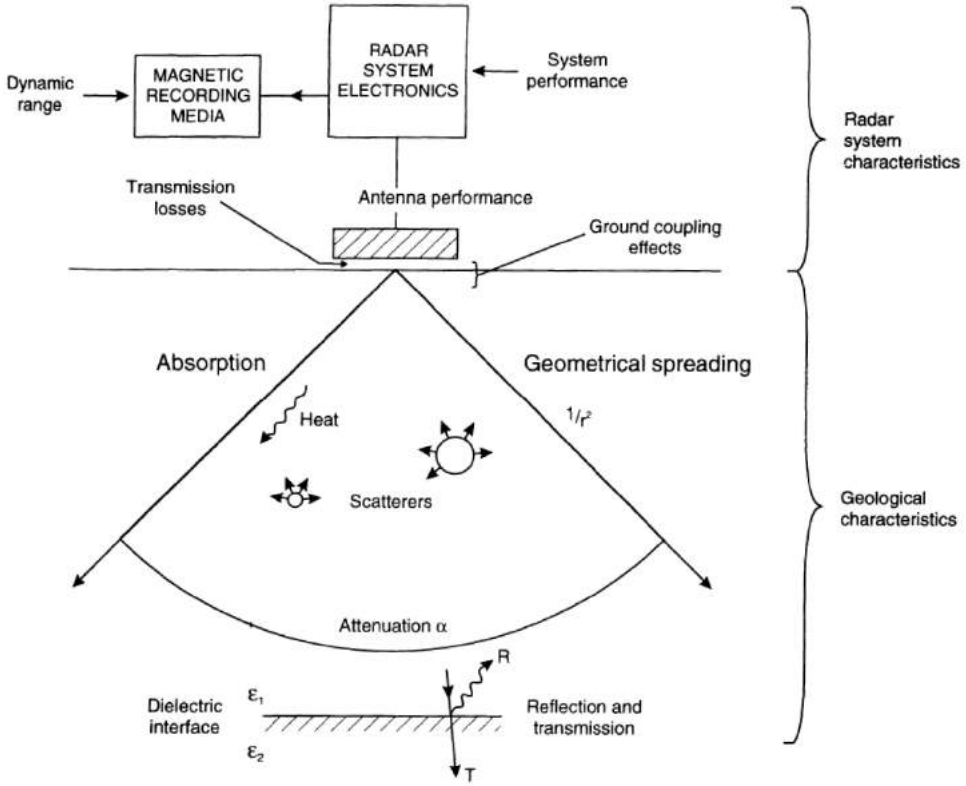

Figure 7.11: Processes that lead to reduction in signal strength (*Reynolds*, 1997)

Energy losses are also induced as a consequence of reflection and transmission losses during each passage through a boundary. The transmitted fractions cannot be registered anymore by the receiving antenna. Due to the missing coupling of the antennas to the ground part of the energy is lost into space. These losses can be summarized as boundary losses.

7.5 Signal Resolution

The successful detection of underground objects or structures is primarily restricted by the resolution of the measurement. This is the ability to distinguish two nearby structures or signals which are temporally close to each other. For the spatial resolution the wavelength λ of the electromagnetic signal is relevant. Are two reflectors separated by more than half a wavelength ($\frac{\lambda}{2}$) they are usually well distinguishable in a radargram. Under very good conditions, the signal resolution can reduce to about one fourth of wavelength ($\frac{\lambda}{4}$). From the relationship of the propagation velocity v with the wavelength λ and the frequency f: $\lambda = \frac{v}{f}$ it is obvious that the smaller the wavelength and the higher the frequency, the higher is also the spatial resolution of the measurement. As mentioned in section 7.4 a higher frequency leads to a shallower penetration depth. Hence, when planning a survey one always has to find am optimal setup for a potentially high penetration depth together with a high resolution of underground structures. Sometimes it is preferable to choose a

deeper penetration depth and a lower resolution if deeper situated structures are to be investigated.

After equation 4.18 an electromagnetic wave travels slower in a wet soil than in a dry soil due to their difference in relative permittivity. This causes that structures can usually be resolved better in wet soils than in dry ones. Contrary, the signal attenuation is higher in wet materials which usually reduces the penetration depth is these measurements.

7.6 Concluding Remarks

GPR is one of the most often applied geophysical measurement techniques. A great advantage is the good applicability under most field conditions. Common offset and multi-channel measurements are fast and allow to efficiently and non-invasively explore large areas at scales ranging from several tens of meters up to a few kilometers. GPR is best suited for taking measurements in low loss materials like sand or gravel since they are well penetrable by radio waves. In fine textured soils like clay or loam or in soils with high electrical conductivity GPR is less applicable since the signals are attenuated too strongly.

8 Site Introduction: ASSESS-GPR

The experiments of this field course are conducted at our experimental field site ASSESS-GPR. This artificial testbed has been built into a former drive-in fodder silo close to Heidelberg in June 2010. Its main purpose is to facilitate the understanding of hydraulic soil processes and further state-of-the-art GPR measurement and modeling methods. The following site description is taken from *Klenk* (2012).

8.1 Construction and basic characteristics

Some pictures taken before and during the construction process can be found in figure 8.4. The testbed is about 20 m long, 4 m wide and approximately 1.9 m deep. Its total surface area has been estimated to 79.94 m^2. The concrete bottom and walls of the structure have been sealed by adding a sturdy polyethylene foil (see picture in figure 8.4c). A complicated but well-defined quasi-2D architecture was designed as a part of the diploma work of *Antz* (2010). This design features three distinct kinds of sand with a gravel layer of about 0.1 m thickness at the bottom. A sketch of this subsurface architecture can be found in figure 8.1. As can be seen in this sketch, there are regions of different complexity with respect to the soil water dynamics and the expected GPR signal evaluation. Ordered by increasing complexity, the following regions can be distinguished:

- a two-layer region (16 m ... 20 m)
- several three-layer regions, in part with swapped layering of the materials (0 m ... 2 m vs. 7 m ... 10 m and 12 m ... 14 m)
- regions with slanted (2 m ... 7 m) and converging reflectors (14 m ... 16 m)
- and, most distinctively, a synclinal structure (10 m ... 12 m)

Since the bottom and the wall of the whole structure have been sealed, precipitation will accumulate at the bottom, leading to a rising water table over time. During normal operations of the test site, the water table is kept at depths between -1.6 and -1 m by pumping water out of the observation well which is located at approximately 18.4 m. If desired, the pumping well can also be used for artificially raising the water table through imbibition. The high saturated conductivity of the additional gravel layer at the bottom of the structure is to equally distribute imbibition or drainage fluxes along the lower boundary during our experiments.

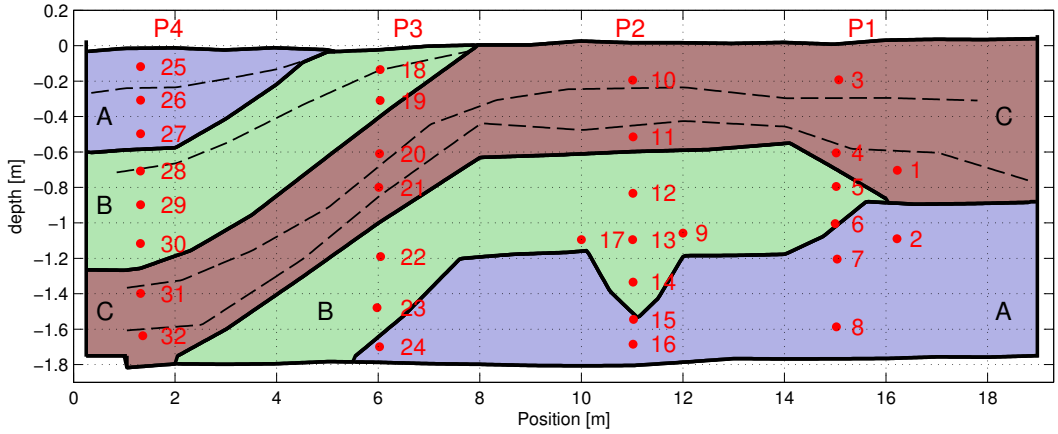

Figure 8.1: Sketch of the structure of the ASSESS-GPR test site. Thick black lines denote layer boundaries between the differently shaded materials, the dashed black lines known compaction interfaces within the same material. TDR sensors are indicated by red dots.

During the building process, the sand was carefully added layer by layer. To ensure the stability of the boundary layers, the sand was compacted with a vibrating machine after each layer addition. Due to the thickness of the different layers, the sand also had to be compacted several times within the same layer, leading to distinct compaction interfaces. The position of some of these compaction interfaces has been explicitly determined; those interfaces are illustrated by the dashed black lines in figure 8.1. The porosity change over these compaction interfaces can give rise to a reflection of the GPR signal, depending on the hydraulic state of the site.
The boundary conditions (e.g. precipitation, air temperatures, water table position) are measured on-site by an automated weather station (see *Antz* (2010) for details). In particular, 32 TDR sensors have been placed in four separate profiles as indicated by the red dots in figure 8.1.
During spring and summer 2015, the ASSESS site has been outfitted with a motorized measurement system which is simply called "field scanner" in the following. This field scanner comprises a measurement bridge which can move automatically up and down the ASSESS site. On this bridge, the antennas can be fixed in several positions allowing the automated acquisition of common offset measurements with differing antenna separations, at different polarizations as well as acquiring CMP measurements automatically at different positions along the ASSESS site.

8.2 Exemplary GPR measurement

A typical example of a multi common offset GPR measurement under quasi-equilibrium conditions (acquired at an antenna box separation of 1.3 m after a dry-spell of approximately four weeks) is shown in figure 8.3. For facilitating the visibility of subsurface structures, the direct wave has been clipped for the two internal channels (INT1 and

Figure 8.2: Morning view of the ASSESS site during a field experiment in November 2015

INT2). In general, the reflections generated by the subsurface interfaces are clearly distinguishable. Most prominent features include the layer boundary between sands B and C, especially including the reflection signal generated by the synclinal structure at 8. . . 10 m. At travel times between 38 and 50 ns, two continuous reflections can be discerned. The first, fainter reflection is most likely generated by the transition to the gravel layer while the second, more prominent reflection is generated by the concrete bottom. Furthermore, there is a comparatively weak horizontal reflection arriving at travel times around 22 ns. This reflection is essentially generated by the top of the capillary fringe and the corresponding transition zone above the water table.

Table 8.1: Effective Brooks-Corey Parameters for the three sands used at ASSESS-GPR, based on the results by *Jaumann* (2012).

	h_0 [m]	λ	K_s [cm h^{-1}]	τ	θ_s	θ_r
A	-0.1621 ± 0.0003	1.40 ± 0.02	30.7 ± 0.1	0.01 ± 0.01	0.3819 ± 0.0002	0.0353 ± 0.0006
B	-0.0961 ± 0.0002	1.35 ± 0.01	461 ± 6	1.07 ± 0.01	0.3198 ± 0.0002	0.0340 ± 0.0004
C	-0.0585 ± 0.0002	3.74 ± 0.04	9.17 ± 0.02	0.05 ± 0.01	0.3494 ± 0.0003	0.0516 ± 0.0002

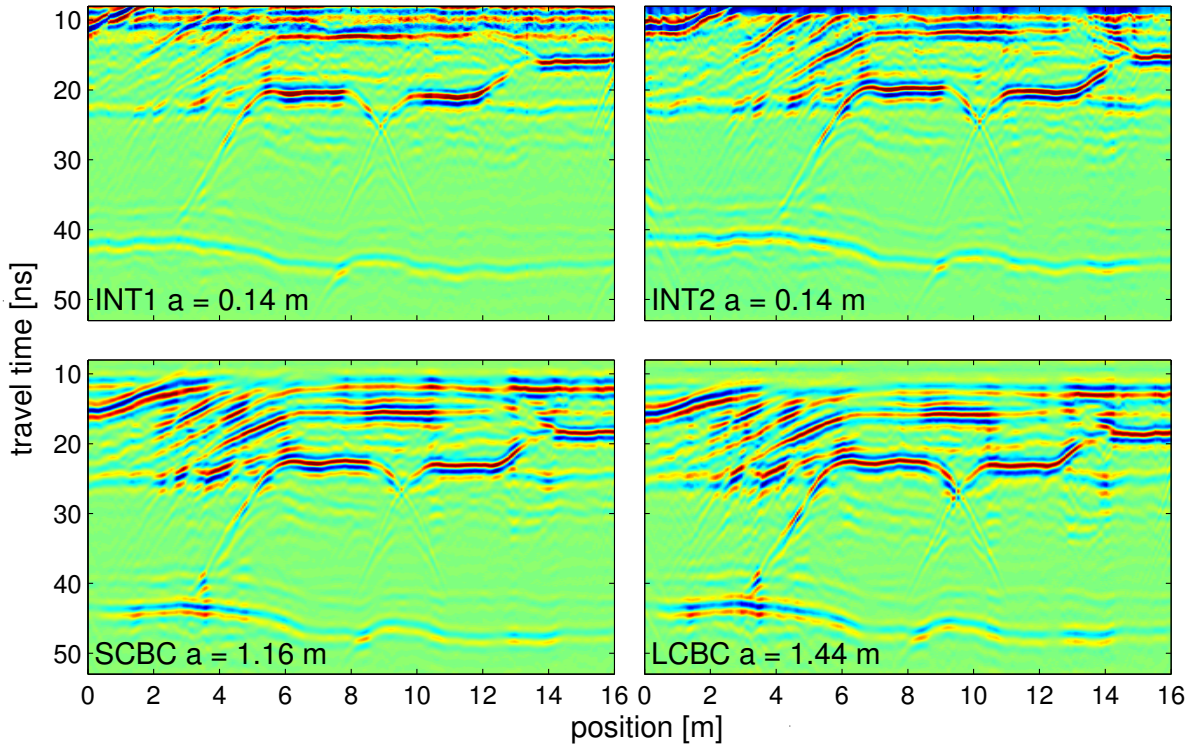

Figure 8.3: Exemplary four channel measurement of the whole ASSESS-GPR site acquired at November 28th 2011 after a long dry spell. Channel designations and the corresponding antenna separations are indicated in each radargram. Channels one and two denote the two internal channels, three and four the long and short crossbox channel, respectively.

8.3 Previous studies at ASSESS-GPR

In recent years, a series of diploma, master and PhD theses have been carried out in connection to the ASSESS site:

The design and the construction process of the ASSESS-GPR site were a part of the diploma thesis of *Antz* (2010).
The water content measurements recorded by the TDR probes have been the basis for the recent diploma work of *Jaumann* (2012), focusing on the estimation of effective hydraulic parameters for the ASSESS-GPR structure. The current best result of an effective parameter set calculated in a recent inversion based on that work are reported in Table 8.1.
A first GPR related study at the ASSESS-GPR site was carried out by *Kühne* (2010), analyzing the temporal variability of soil water content as measured with multichannel GPR between June and September 2010. Subsequently, this analysis was extended by another time-series measured between December 2010 and April 2011 in the framework of the thesis of *Bogda* (2011), focusing on optimizing the measurement setup for the multichannel analysis. GPR data acquired at the ASSESS-GPR site have been the basis for the novel inversion approach for surface GPR data which has been presented by *Buchner*

et al. (2012).

The well-controllable nature of the ASSESS-GPR site provides excellent conditions for studying the GPR response to different hydraulic states of a field site. Such different hydraulic states can be simulated by varying the water table through imbibition and drainage into and from the structure at the observation well. A first description of the GPR response to experiments with fluctuating water tables has been recently provided by *Seegers* (2012). These experiments were also the foundation for the diploma thesis of *Dagenbach* (2012), who performed a detailed numerical analysis of the GPR response to the transition zone above the capillary fringe. Comparing the time-lapse measurements acquired during the experiments to the results of numerical simulations, an appropriate soil hydraulic parametrization has been identified by *Dagenbach et al.* (2012). *Keicher* (2013) carried out a series of GPR measurements at the ASSESS site for detailed investigation of the precision and accuracy of our instruments. Most recently, this was expanded upon by *Piepenbreier* (2015), focusing on detailed investigations of amplitude and frequency behavior of different GPR signals recorded at the ASSESS site.

In case you are interested in expanding this list, please feel free to contact us! :-)

8.4 Alternate field site: Grenzhof

In case the ASSESS site is unavailable for practical course measurements, the experiments will be conducted on an alternate field site close by, which is called the "Grenzhof–site". This is a stretch of formerly agriculturally used land which our group has been leasing continuously for the last 15 years. The site is equipped with an automated weather station. Several soil profiles have been instrumented with TDR and soil temperature probes measuring continuous time-series for over a decade. Experiments we have been carrying out at this site were aimed at understanding the nature soil water and contaminant flow in the vadose zone as well as the energy balance at the soil-atmosphere boundary. Before the ASSESS site had been built, most of our development of GPR methods have been taking place here as well.

(a) ASSESS-GPR site before construction. View towards start of GPR profiles

(b) ASSESS-GPR after smoothing of the ground. View towards end of GPR profiles

(c) ASSESS-GPR after installation of the pond liner

(d) ASSESS-GPR during construction

(e) GPR measurements during imbibition and drainage experiment

(f) GPR measurements during imbibition and drainage experiment

Figure 8.4: Pictures from the ASSESS-GPR site. The top row shows the structure before, the middle row during construction. The bottom row shows the GPR measurement process during the imbibition and drainage experiments similar to what we will be conducting in the framework of this field course

9 Experiments

9.1 Structure and aims of the experiments

The main goal of the taking part in the experiments of this field course is to achieve a thorough understanding of the principles and applications of two geophysical measurement methods that have found wide-spread use for determining soil moisture contents.

The usual practical course comprises two parts:
For part A, TDR measurements are executed in the laboratory at the Institute of Environmental Physics. The aim of this part is to record and interpret reflected signals of electromagnetic waves in several media under different conditions.
Measurements for the part B will be carried out at one of our test sites in the vicinity of Heidelberg, where you will head together with your supervisor on the second day. At that site, several different GPR measurement methods will be used. Since July 2015 this will normally be the ASSESS site, as described in detail in chapter 8. Also, some TDR measurements may be recorded for comparison. The evaluation of all these measurements and their comparison fill the third day of this practical course.

Please be advised that you are handling scientific equipment which is worth about 100.000 €. Servicing a broken GPR connecting cable costs us about 500 €. The TDR100 device costs around 4000 € to replace due to the expensive high frequency generator. In light of these numbers, please execute extreme caution while handling the instruments.

Especially if you are executing measurements with the new field scanner on the ASSESS site, utmost care is to be taken, as there are not all software based security checks in place yet. Not paying attention will most definitively lead to potentially very expensive screw-ups. If anything seems to be difficult to put together, ALWAYS stop and ask.

9.2 Guiding questions

Before starting with the experiments you should at least be able to answer the following questions:

Theoretical Questions

- How do electromagnetic waves propagate in matter? What parameters are needed to describe this propagation?
- Which processes lead to energy dissipation of an electromagnetic wave propagating in a certain medium?
- Which regions of the electromagnetic spectrum are used for measuring relative permittivities and why?
- How and why can one determine soil water content from relative permittivity?
- What are the basic principles of Time Domain Reflectometry? How can relative permittivities be determined from TDR measurements?
- What are the fundamental principles of Ground-penetrating Radar? How can GPR measurements be employed for determining relative permittivities?

Practical Questions

- What kind of different methods for GPR measurements are there and what are the (dis-) advantages of these methods?
- Which quantities can be determined by the different GPR measurements?
- With which method can the temporal offset t_{air} (equation 7.8) be measured for the different channels?
- What are the similarities and differences between GPR and TDR based measurements?

9.3 Laboratory measurements using TDR

As stated above, the first part of the experiments will be carried out in the laboratory at the Institute for Environmental Physics and will mainly deal with TDR measurements.

9.3.1 Basics: Performing TDR measurements

The TDR measurements in this practical course are acquired using a TDR100 instrument (see fig. 9.1), manufactured by Campbell Scientific Inc. This TDR100 instrument is a computer controlled reflectometer, where the program PCTDR is used for data acquisition. This program also allows for a graphical representation of the reflected signal.

For getting started, please execute the following steps:

1. Connect the TDR100 to the measurement laptop via the com-port.
2. Connect the TDR100 to the battery. Please use the respective power cord. Caution! Ensure using the right polarity when connecting the plugs (black plug $\hat{=}$ negative polarity).
3. Boot the measurement laptop, just klick on *ok* if asked for a password.
4. Open the data acquisition program PCTDR via the link provided on the desktop.

At first you should get thoroughly acquainted with the measurement setup. To this end, please connect one of the provided TDR-sensors to the TDR100, activate the button *continuous update* and start a measurement.

Figure 9.1: The TDR100 instrument

You should now conduct a first qualitative analysis of the form of the signal in different media – like air, water or sand. *Print out at least one TDR trace in air and one in water for your report.*

9.3.2 Calibration of TDR sensors

For a quantitative analysis (which you are **not** obliged to do, a qualitative analysis is sufficient) of all subsequent measurements, the TDR sensors would have to be to be calibrated first.
This would be achieved by recording two-way traveltimes (compare chapter 6.2) of the signal in at least two different media with different but well defined permittivities, which allows to associate every measured travel time uniquely with the respective permittivity based on equation 6.1. The best way for TDR calibration here is to use water and air, as these two media can be considered to represent the two *extreme cases* for moisture content in natural soils. Normally, you would record five traces (*why more than one?*) in air and and then five more completely submerged in completely desalinated water (*VE-Wasser*). However, since you will not use the provided sensor for quantitative measurements in the field, you can resort to just recording one trace in air and one in desalinated water. Make sure, that the whole trace is visible in the window of PCTDR. If this is not the case, adjust the axes accordingly. Saved traces will have the same resolution as pictured in the program window.
From what you know about measuring water content with TDR sensors, would you need to record any further parameters for achieving a quantitative water content value?
As you are not obliged to do a quantitative analysis of the TDR measurements[1], it is sufficient if you just record the trace in air and in desalinated water and explain the form and the reasons for the differences.

Write down your program settings like *Start, Length* and v_p so you can calculate the resolution of the x-axis during the evaluation. Roughly estimate from the measured traces the permittivity of water and air. Compare to known values from literature to make sure all settings are right.

9.3.3 Measurement: TDR signals from a sand column

In this part of the experiment, the provided TDR sensor will be used to qualitatively measure different water contents in an approximately 40 cm high sand column (if you use a TDR sensor with 0.3 m length), the according experimental setup is pictured in figure 9.2. The water table in this sand column can be tuned to different heights, therefore inducing different water contents which can be measured with a TDR sensor.

Please read this section and answer the questions before starting the experiment!

At first, insert the provided TDR sensor with 30 cm rod length vertically into the initially dry soil column. Please take extra care not to introduce any air gaps along the rods while inserting the sensor, as this will severely impair the measurement and could yield completely worthless results. Please ensure that the PCTDR-window shows the complete

[1] This implies the calculation of the soil water content from the measured TDR trace.

Figure 9.2: Overview of the measurement setup for the soil column

signal over the whole measurement process[2]. You may start tuning the PCTDR-window using the following parameters: *start: 3.0, length: 5.0*. Be aware that this window depends on the length of the probe and the cable.
Then the water table is to be risen slowly from the bottom of the soil column until the water level is approximately 5 cm below the surface. This can be done by adjusting the height of the water container. Hanging the water container higher will raise the water table in the column due to the increase of hydrostatic pressure. Record one TDR trace after every rise of the water table of 5 cm and approximately 2 minutes. The final trace should be recorded after the saturation front in the column is approximately 5 cm below the surface and the system has been equilibrating for approximately 15 minutes. Then, establish the water level to the 2 cm above the top of the porous plate at the lower end of the sand column, so that the water can slowly flow back out of the column. Again, record one TDR-trace after every 2 minutes.

Make sure that you stop the outflow of the water before the porous plate at the bottom of the sand column runs dry!

After finishing your experiments, get the TDR sensor out of the sand column and put the wet sand in an appropriate box with the help of your tutor. Be reminded that you are working in a laboratory. Please clean it accordingly. No grain of sand must be on the tables and the floor has to be swept at minimum! You will find scoop and brush below the wash basin.

[2]Record one trace in water and one in air to evaluate the extreme cases.

Guiding Questions:

- Give three difference between the recorded traces in air and in water.
- Describe the expected changes, if you would measure with different TDR probes (feel encouraged to do so).
- Sketch the expected water content distribution over the height of the column over time for the whole experiment.
- Describe the expected traces you will measure.

Remarks on the expected evaluation

The following evaluation of your measurement data is expected:

1. Plot the measured traces for water and air in one figure. Please shift them such that the reflection at the probe head is at the same position. You may also measure with different TDR probes and explain the differences in the measurement data.
2. Plot all the measured traces during the rise of the water table in the sand column in one figure. Please use different colors for each trace. It is suggested to use ascending colors with measurement time[3].
3. Create the same plot for the drainage part of the experiment.

9.3.4 Measurement: Assessing the Influence of conductivity

As has been described in section 6.3, the shape of the TDR signal is influenced by the electric conductivity of the measured medium along the TDR sensor rods. In this part, this influence is to be qualitatively assessed. To get a feeling for this effect, a set of TDR traces is to be recorded in water exhibiting different salt concentrations as follows:

1. Fill a bucket with 20 l of completely desalinated water.
2. Connect a TDR sensor with 20 cm rod length to the TDR100 and adjust the following settings of the PCTDR software under the menu *waveform*: *start = -2.00*, *length = 202.00*.
3. Record the TDR signal when the sensor is held vertically in the bucket.
4. Then successively add 2 g of salt to the bucket, stir thoroughly until complete dissolution and record a TDR trace afterwards, until a total of 10 g have been dissolved. You should have recorded six TDR traces for this part of the experiment.

[3] You could choose e.g., 0 min → red, 2 min → orange, 4 min → yellow, 6 min → green, ...

9.4 Field measurements

Under normal circumstances, the field experiments will be executed at the ASSESS testsite close to Heidelberg. In July 2015, the ASSESS site has been outfitted by a field scanner. You will be among the very first to actually use this system for acquiring GPR data. Hence, again: Please take utmost care in handling the system.

As the field scanner has just been installed and is still being tested, the specific type of measurements which we can execute will be determined dynamically and is subject to weather conditions.

9.4.1 Planning your measurement

As a prerequesite, please be prepared to answer / discuss the following aspects of these experiments. There may be no right or wrong answer, but most of these questions are exactly the questions we have to ask ourselves when designing our own experiments:

- What would you expect to be able to learn from a single GPR measurement at the ASSESS site about the properties of the subsurface?
- In principle, what could we - provided a perfect measurement setup - learn more about subsurface hydraulics by monitoring subsurface hydraulic dynamics?
- What is the additional information we can gain from CMP measurements with respect to common offset data?
- How would you decide on an appropriate antenna separation?
- We have different instruments available. Specifically, we have access to GPR instruments with center frequencies of 100, 200, 400, and 500 MHz als well as to dual frequency antennas with centerfrequencies of 200 and 600 MHz. If you could decide for a specific instrument - given the dimensions of the field site and the nature of these experiments - which instrument would you pick? For supporting your decision, please calculate the dominating wave lengths for the respective frequencies for (i) wet soil ($\theta \approx 0.2$ and (ii) dry soil ($theta \approx 0.05$).
- What is more desirable: High temporal resolution but less spatial coverage or more extended spatial coverage at the expense of lower temporal resolution?

9.4.2 Measurements you will need for evaluation

If everything works as planned, please make sure to have recorded at least the following measurements and copied them somewhere for your specific evaluation:

- Two eight channel, common offset measurements along the long axis of the ASSESS site recorded at the same polarization with three different antenna separations.
- Three different CMP measurements recorded at characteristic locations along the ASSESS site. At least one of them should be coincide with the location of one of the preinstalled profiles of TDR sensors.
- Made a readout of today's weather station data, especially including the TDR measured water contents.

If time is left think about additional measurements like:

- A common offset measurement recorded with one of the two previous antenna separations but differing polarization.
- WARR measurements at the locations of the CMP measurments
- Measurements at different distances to the silo wall

For evaluation purposes, please make sure that you

- have made a detailed sketch of every antenna setup you have been using. Note down the serial numbers of antennas and cables and note the direction the antennas have been facing.
- have measured and noted all employed antenna separations during CO measurements as well as the initial antenna separations for CMPs.
- have noted the starting and end points of the COs as well as the locations and shotpoints of CMPs.
- have noted the transmitter-receiver sequence for the channels as displayed in the measurement software K2fastwave.

9.4.3 Executing GPR measurements with automated field scanner

Setup

- carry whole equipment to ASSESS site:
  - field scanner control box
  - 2 antennas 200/600 MHz
  - GPR control unit
  - GPR cable (black, ≈ 3 cm diameter)
  - LAN cable
  - 12 V battery, battery cable
  - wheel cable
- install field scanner control box to bridge and connect all already installed cables to it
- install both antenna boxes at FS bridge
- connect with installed GPR cable and additional brought GPR cable both antennas to GPR control unit: CU "Ant. 1" to "IN" of antenna 1, "OUT" of antenna 1 to "IN" of antenna 2
- write down serial numbers of antenna 1 and 2
- connect GPR CU to battery and to FS control box
- connect CU "Wheel" to "IDS" at FS control box
- connect CU "LAN" to "radar LAN" at FS control box
- connect power to plug in at ASSESS wall
- switch on CU (red light is shining)

GPR settings

- connect red LAN cable to Toughbook, turn it on
- start program K2FastWave
- click on configuration

- choose appropriate profile like "2 Ant 8CH 200/600MHz remote" (for usage of external measurement wheel: "2 Ant 8CH 200/600MHz wl06"
- control and write down measurement window, wheel integration, number of samples
- ok
- click on all 8 measurement windows to adjust and write down degree factor ("offset"). The measurement window of all channels should include the direct wave signal and the bottom reflection. (typical values: CH1-CH4: 0°, CH5/CH7: 334°, CH6/CH8: 30 °)
- start calibration
- advanced settings → autostacking
- new acquisition (name *FPyearmonthday*)
- advanced settings →wheel
- adjust field scanner movement as planed
- start scan→ measurement will be executed when field scanner moves
- click stop scan + save scan to save measurement
- always write down at least profile number, type of measurement and movement range of field scanner for analysis

Field Scanner settings

- start *Putty* via desktop icon
- set up ssh connection to IP: 192.168.200.201, port 22
- username: geier, pw: bophy
- *sudo ipython*
- *cd ./fieldscannerRPI3/build/src/*
- executing one of the python scripts by *%run scriptname.py* will start movement and radar measurement immediately, so make sure GPR measurement is prepared (start scan at K2FastWave) and movement of scanner is possible without causing any damage at equipment or people
- a radar trace is measured every 2 cm during the field scanner movement

- provided scripts:
  - *scannerPy_CO1.py* : movement of large field scanner bridge in direction 1 to installed end switch at slide
  - *scannerPy_CO2.py* : movement of large field scanner bridge in direction 2 to installed end switch at slide
  - *scannerPy_CMP1.py* : movement of antennas at small field scanner bridge in direction 1 to installed end switch
  - *scannerPy_CMP2.py* : movement of antennas at small field scanner bridge in direction 2 to installed end switch
- stop measurement: press "E", *runMonitor(StopScanner(),scanner)*
- automated movement of field scanner is still under development. Thus unexpected errors are always possible. During scanner movements at least one person **always** has to stay next to the Toughbook and emergency stop switch to stop movement if required.

10 Evaluation

The evaluation of the experiments carried out in this practical course should at least include a detailed treatment of the the following points.

10.1 Evaluation of the TDR measurements

10.1.1 Qualitative description of TDR signals

Describe the qualitative characteristics of the TDR signal and its shape when measured in different media. Discuss in detail the traces acquired in air and water. What are the key differences and similarities and how can they be explained?

10.1.2 TDR signals from the sand column

Graphically represent the TDR traces while the water gauge in the sand column was on the rise. Discuss the changes of the signal characteristics. Determine the water content from measurements while the gauge was on the rise and on the fall. Plot the respective water contents vs. the according heights of the water gauge. What conclusions can be drawn from this diagram?

10.1.3 Assessing the influence of conductivity

Plot all recorded traces into a joint diagram and label each signal accordingly. What is the influence of increasing electrical conductivity on the shape of the TDR signal? What is the maximum salt concentration at which water contents could still be safely calculated? How would you go about extracting quantitative information on electrical conductivity from this data. Would a two-point-calibration suffice?

10.1.4 TDR field data

Please calculate the water content distribution of the ASSESS site as measured at the day of your field measurements by the automated weather station. For details on how to, please ask. If you should come up with one single average water content for the whole profile, how do you have to average these TDR-derived water content values?

10.2 Evaluation of the GPR field measurements

GPR data are evaluated by a dedicated software package "MatlabGPR" which is a matlab based class of different methods. For each evaluation step we provide you with a dedicated script which you may use and adjust at will.

10.2.1 Evaluation of measured data

Please copy all measurement data into the following subfolder of your current home folder, replacing the "YYMMDD" with the appropriate date of your field experiment: "∼/YYMMDD/fielddata/0_data/<YYMMDD>.MIS/LID_acq1". (

For the evaluation, please select:

- one 8-Channel CO measurement recorded with normal polarization setup
- a corresponding second 8-Channel CO measurement recorded with the same normal polarization setup but a different antenna separation
- if measured:One 8-Channel CO measurements recorded with the same antenna separation but in different polarization

All selected profiles should be either measured from 0 to 19 m or in reverse direction. Furthermore, each group should select three CMP profiles you have recorded, at least one of which should coincide with one of the preinstalled TDR sensor profiles on the site.

All matlab scripts you will be using for evaluation can be found in the folder: "∼/YYMMDD/fielddata/1_matlab/".

Please **think** about and discuss the following tasks, then carry out the following evaluations:

Overall data interpretation - common offset

- First, plot all radargrams from your chosen 8-CH CO measurements (three antenna separations, all polarizations), as well as the 8-CH radargrams from all three of your CMP measurements using the script "Script1_plot_8CH.m". This should yield plots, which are saved into the folder "3_plots".

  If you want to look at more details from a single channel radargram with minimal evaluation effort, consider using the script "Script0_quickplot_1CHCO.m", plotting a single radargram into a file. Another way for looking at details more closely is using the script "Script1b_plot_1CH_wtraces.m", which allows you to plot a number of radargrams (which you put into the variable "GPRfiles") with extra traces alongside it.

- For the normally polarized CO measurement, answer the following questions:

  - Which channel has been measuring at which frequency?

  - Which channels are internal or crossbox channels?

  - You know the TR sequence from the measurement software and the antenna box setup you used during the measurements. Can you decide the layout of the antennas? Which channels have the longest antenna separations? Given your knowledge about the antenna box separation and the internal antenna separations (600 MHz antennas: $a_{int} = 0.09\ m$, 200 MHz antennas: $a_{int} = 0.23\ m$, what are the antenna separations for each channel? You will need these values for calculating water contents from the evaluation of the bottom reflection in these radargrams later on! Also, the CMP evaluation depends on knowing the correct initial antenna separation. If you are not sure of your result, ask!

  - Compare the measurements acquired at different antenna separations. What kind of differences should you expect? Do you see any differences?

  - Compare the measurements acquired at different polarizations. What kind of differences should you expect? Do you see any differences? Why?

  - What kind of signals can you discern from the data? Please identify all layer reflections, the direct wave and the signal from the capillary fringe above our water table. Any other interesting features?

  - Can you directly estimate the water table depth from observations of the capillary fringe reflection? Make a couple of plots with traces at different positions (using "Script1b_plot_1CH_wtraces.m"), choosing appropriate channels from your CO measurement and discuss potential differences you may observe for the capillary fringe reflection in different materials. Compare with the measured water table depth during the GPR measurements.

Overall data interpretation - common midpoint data

Use the script "Script2a_quickplot_3CMPs.m" for making two additional plots: (i) plot channels 5 and 6 for all three of your chosen CMP radargrams and (ii) do the same for channels 7 and 8.

- For the three CMP measurements, answer the following questions:
  - What is the nature of the signals of the first four channels (as plotted in the original 8CH-radargrams)?
  - For channels 5-8: what kind of signals can you identify? Have you measured the air wave / ground wave / layer reflections (how many?) / refracted waves?
  - What are the differences observed between your three chosen CMP radargrams? Can you relate these differences to the known subsurface structure of the ASSESS site?
  - How do the signals of the two different frequencies compare in each case?

Evaluation for water content

Furthermore, you should evaluate obtained data for water content:

First, use the script "Script2b_evaluate_3CMPs.m" to fit (i) the direct ground wave and (ii) the bottom reflection and calculate the respective averaged water contents for your three chosen CMP measurements. Make sure (i) that you have input the right starting antenna separation for each channel ("importpars.antsep") and (ii) that you use the same feature for picking, at best the central minimum feature (*why?*). As before, execute the script two times, using first channels 5 and 6 and then channels 7 and 8.

Finally, use "Script3_eval_bottomrefl_1CHCO.m" to evaluate the bottom reflection for each of the eight channels in your originally chosen normal setup CO measurement for water content. Make sure that you provide the correct antenna separation for each channel. This script assumes a constant depth of the bottom of the ASSESS site of 1.9 m. In this case, you have to provide the respective air wave travel time for each channel for time zero correction. Each group should use its own measured radargram containing the air wave calibration. In the end, you should find eight .mat-files containing both water content and permittivity in the folder "2_outputs". Plot all results for the water contents into a single diagram and discuss potential differences you find for the different channels.

10.2.2 Comparison between methods and to TDR data

Last but not least, you should discuss and assess the precision and accuracy of the water content results derived from different methods. First, compare the CO results to the results obtained by CMP fitting and assess and explain potential differences between the two methods. Then compare the results to the TDR derived values. Find a way to efficiently compare the result for the CMPs acquired close to TDR sensor profiles with the water contents derived from these TDR profiles. How well do the results match? Is this what you would have expected?

Bibliography

Antz, B. (2010), Entwicklung und Modellierung der Hydraulik eines Testfeldes für geophysikalische Messungen, Diploma thesis, Heidelberg University.

Birchak, J. R., C. G. Gardner, J. E. Hipp, and J. M. Victor (1974), High dielectric constant microwave probes for sensing soil moisture, *Proceedings of the IEEE*, *62*(1), 93–98, doi:10.1109/PROC.1974.9388.

Bogda, F. (2011), Untersuchung der Bodenwasserdynamik mit Mehrkanal-GPR, Staatsexamensarbeit, Heidelberg University.

Brooks, R. H. (1966), Properties of porous media affecting fluid flow, in *Journal of the Irrigation and Drainage Division, Proceedings of the American Society of Civil Engineers*, vol. 92, pp. 61–88.

Brovelli, A., and G. Cassiani (2008), Effective permittivity of porous media: a critical analysis of the complex refractive index model, *Geophysical Prospecting*, *56*(5), 715–727, doi:10.1111/j.1365-2478.2008.00724.x.

Buchner, J. S., U. Wollschläger, and K. Roth (2012), Inverting surface GPR data using FDTD simulation and automatic detection of reflections to estimate subsurface water content and geometry, *Geophysics*, *77*(4), H45–H55, doi:10.1190/geo2011-0467.1.

Dagenbach, A. (2012), Untersuchung der hydraulischen Bodeneigenschaften durch GPR: Analyse der Kapillarsaumreflexion durch numerische Simulationen, Diploma thesis, Universität Heidelberg.

Dagenbach, A., J. S. Buchner, P. Klenk, and K. Roth (2012), Identifying a soil hydraulic parameterisation from on-ground GPR time lapse measurements of a pumping experiment, *Hydrol. Earth Syst. Sci. Discuss.*, *9*, 9095–9117, doi:10.5194/hessd-9-9095-2012.

Drude, P. (1900), Zur Elektronentheorie der Metalle, *Annalen der Physik*, *306*, 566–613.

Gerhards, H. (2008), Ground penetrating radar as a quantitative tool with applications in soil hydrology, Ph.D. thesis, Heidelberg University, http://katalog.ub.uni-heidelberg.de/titel/66617610.

Heimovaara, T., A. Focke, W. Bouten, and J. Verstraten (1995), Assessing temporal variations in soil water composition with time domain reflectometry, *Soil Sci. Soc. Am. J.*, *59*, 689–698.

Jackson, J. D. (2006), *Klassische Elektrodynamik*, 4th revised version ed., 358 ff pp., Walter de Gruyter.

Jaumann, S. (2012), Estimation of effective hydraulic parameters and reconstruction of the natural evaporative boundary forcing on the basis of TDR measurements, Master thesis, Heidelberg University.

Kaatze, U. (1989), Complex permittivity of water as a function of frequency and temperature, *Journal of Chemical and Engeneering Data*, *34*, 371–374.

Keicher, V. (2013), Quantitative untersuchungen zur stabilität von georadarsignalen bei messungen von assess-gpr, Master thesis, Universität Heidelberg.

Klenk, P. (2012), Developing ground-penetrating radar for quantitative soil hydrology, Ph.D. thesis, Heidelberg University.

Kühne, A. (2010), Experimentelle Untersuchung der zeitlichen Variabilität des Bodenwassergehalts mit GPR, Staatsexamensarbeit, Heidelberg University.

Mualem, Y. (1976), A new model for predicting the hydraulic conductivity of unsaturated porous media, *Water Resources Research*, *12*(3), 513–522, doi:10.1029/WR012i003p00513.

Piepenbreier, N. (2015), Quantitative untersuchung des amplituden- und frequenzverhaltens von gpr antennen unterschiedlicher frequenzen, Master thesis, Universität Heidelberg.

Reynolds, J. (1997), *An introduction to applied and environmental geophysics*, John Wiley & Sons.

Richards, L. A. (1931), Capillary conduction of liquids through porous mediums, *Physics*, *1*(5), 318–333, doi:10.1063/1.1745010.

Robinson, D., S. Jones, J. Wraith, D. Or, and S. Friedman (2003), A review in dielectric and electrical conductivity measurements in soils using time domain reflectometry, *Vadose Zone J.*, *2*, 444–475.

Roth, K. (2012), *Soil Physics Lecture Notes*, Heidelberg University, Germany.

Roth, K., R. Schulin, H. Fluehler, and W. Attinger (1990), Calibration of time domain reflectrometry for water content measurement using a composite dielectric approach, *Water Resources Research*, *26*(10), 2267–2273.

Seegers, C. (2012), Experimentelle Untersuchung der Bodenwasserdynamik mittels Georadar, *in German*, Diploma thesis, Heidelberg University.

Van Genuchten, M. (1980), A Closed-form Equation for Predicting the Hydraulic Conductivity of Unsaturated Soils, *Soil Science Society of America Journal*, *44*(5), 892–898, doi:10.2136/sssaj1980.03615995004400050002x.